N-terminal mutants of human apolipoprotein A-I: structural perturbations associated to protein misfolding

Gisela M. Gaddi[1,2], Romina Gisonno[1,2], Silvana A. Rosú[1,2], Lucrecia M. Curto[3], Esteban E. Elías[1,#a], Eduardo D. Prieto[4], Guillermo R. Schinella[2,5], Gabriela S. Finarelli[1], M. Fernanda Cortez[1], Nahuel A. Ramella[1,2,¶,*], M. Alejandra Tricerri[1,2,¶*]

Short title: Structural perturbations involved in amyloidosis from N-terminal mutants of human apolipoprotein A-I

[1] Instituto de Investigaciones Bioquímicas de La Plata (INIBIOLP), CONICET, La Plata, Buenos Aires, Argentina

[2] Facultad de Ciencias Médicas, Universidad Nacional de La Plata, La Plata, Buenos Aires, Argentina

[3]Departamento de Química Biológica e Instituto de Bioquímica y Biofísica, Facultad de Farmacia y Bioquímica, Universidad de Buenos Aires, Buenos Aires, Argentina

[4]Instituto de Investigaciones Fisicoquímicas Teóricas y Aplicadas (INIFTA) Universidad Nacional de La Plata-CONICET, La Plata, Buenos Aires, Argentina

[5]Comisión de Investigaciones Científicas, Pcia de Buenos Aires, La Plata, Argentina

[#a] Current Address: Laboratorios de Inmunología Oncológica. Instituto de Medicina Experimental (IMEX)-CONICET-ANM, CABA, Argentina.

*Corresponding author: E-mail: 1) aletricerri@yahoo.com (MAT); 2) nramella@gmail.com (NAR)

¶ These authors collaborated equally on the present work

Abstract

Since the early description of different human apolipoprotein A-I variants associated to amyloidosis, the reason that determines its deposition inducing organ failure has been under research. To shed light into the events associated to protein aggregation, we studied the effect of the structural perturbations induced by the replacement of a Leucine in position 60 by an Arginine as it occurs in the natural amyloidogenic variant (L60R). Circular dichroism, intrinsic fluorescence measurements and assays of binding to ligands indicate that L60R is more unstable, more sensitive to proteolysis and interacts with sodium dodecyl sulfate (a model of negative lipids) more than the protein with the native sequence and other natural variant tested, involving a replacement of a Trytophan by and Arginine in the amino acid 50 (W50R). In addition, the small structural rearrangement observed under physiological pH leads to the release of tumor necrosis factor α and interleukin-1β from a model of macrophages. Our results strongly suggest that the chronic disease may be a consequence of the loss in the native conformation which alters the equilibrium among native and cytotoxic proteins conformation.

Introduction

Human apolipoprotein A-I (apoA-I) is the main protein associated to high density lipoproteins (HDL). It is synthesized in liver and intestine and both the liver and the kidney are the major sites of its catabolism. Its multiple functions as lipid transport, endothelial homeostasis and inhibition of inflammatory pathways [1][2][3] could however be counter balanced by the presence of single point mutations which could, by not yet completely known pathways, induce its misfunction, increased clearance rate or its tendency to aggregate [4][5]. Hereditary apoA-I amyloidosis has been described since 1969, and is characterized by specific deposits of natural variant proteins within organs, in a pattern which is dependent on the mutation in the protein sequence. From the more than 20 known natural variants, almost half result from substitutions between amino acids 26 and 107, and involve with different severity hepatic and kidney failure. Instead, a “hot spot” affecting residues 173-178 was described, in which variants are especially associated to cardiac, skin and testis damage. The reasons for the different deposit patterns are still unknown but may be the consequence of long term seeding of misfolded proteins that yield a final fibrillar conformation.

The first identified apoA-I natural mutant was the result of a substitution of a Glycine by an Arginine in position 26 from the native sequence (Gly26Arg, in the abbreviated nomenclature G26R), inducing in patients peripheral neuropathy, peptic ulcer, and nephropathy [6]. The next mutations described in the N terminus of apoA-I were Trp50Arg (W50R) [7] and Leu60Arg (L60R) [8]. These variants show similarities with G26R: in each, a neutral residue is replaced by an Arginine thus increasing by one the positive net charge, and amyloid fibrils isolated from the tissues consist of the N-terminal fragments of the variant apoA-I.

As a difference from other hereditary amyloidosis, in which renal failure occurs mainly due to glomerular protein deposits [9][10], apoA-I associated disease is mostly characterized by amyloid retention in the medullary interstitium and/or vasculature, which is probably a reason for its misdiagnosis [11][12]. Only rare exceptions were observed within a few mutants including W50R, in which amyloid deposits were found in glomeruli, either confined [13], or expanded to medulla. Previous works from our and other groups have demonstrated that the single point mutations described for apoA-I decrease the marginal protein stability and elicit the tendency to aggregate; even though the conformational shift in the variants is usually subtle under physiological pH and low concentration, it could also induce alterations of the binding to ligands or the eliciting of pro-inflammatory cellular events [14][15]. In order to extend the knowledge about structural motifs that could be involved in apoA-I aggregation and pathogenicity, we herein studied and described the structural initial events that could result in high yield of misfolded conformations in the pro amyloidogenic variant L60R.We compared this mutant behavior with the Wt and with W50R, which is involved in renal amyloidosis but with a relative different aggregation clinical profile. This last mutant served as good comparison as some structural characterizations were already performed by Gursky and colleagues[16][17].

Materials and methods

Materials

Reagents purchased from Sigma-Aldrich (St Louis, MO) comprise the following: matrix metalloproteinase-12 (MMP-12, Catalytic Domain), Phorbol 12-myristate 13-acetate (TPA), Trypsin, Guanidine hydrochloride (GdmCl), sodium

dodecyl sulfate (SDS), thioflavin T (ThT), polymixin B; 1,2-dimyristoylsn-glycero-3-phosphatidylcholine, (DMPC) was from Avanti Polar Lipids (Alabaster, AL). IMAC Sepharose 6 Fast Flow Resin was acquired from GE Healthcare Bio-Sciences AB, Uppsala, Sweden). The glycosamine glycan Heparin from bovine intestinal mucosa (average molecular weight 15 kDa) was from Northia (BA, Argentina). From Invitrogen (Carlsbad, CA) we obtained 4,4'-dianilino-1,1'-binaphthyl- 5,5'-disulfonic acid, dipotassium salt (Bis-ANS). Isopropyl-β-D-thiogalactoside (IPTG) was purchased to Thermo Scientific (Waltham, MA). All other reagents were acquired with the highest analytical grade.

Methods

Cloning, expression, and purification of wild-type (Wt) W50R and L60R mutants of apoA-I

A cDNA template containing human Wt apoA-I sequence was used in order to introduce the required single point mutations. This construct was inserted into a pET-30 plasmid (Novagen, Madison, WI), allowing the expression and purification of the apoA-I variants fused to an N-terminal His-Tag peptide [18]. The mutants W50R and L60R were obtained by the Quick change method (Stratagene, La Jolla, CA). Primers were as follows:

For W50R: Sense 5'-agctccttgacaacagggacagcgtgacc-3'

Antisense 5'-ggtcacgctgtccctgttgtcaaggagct-3'

For L60R Sense 5'-caccttcagcaagcggcgcgaacagctcg-3'

Antisense 5'-cgagctgttcgcgccgcttgctgaaggtg-3

In order to further remove this N terminal peptide, an Asp—Pro sequence involving amino acid residues 2 and 3 was previously generated to allow specific chemical cleavage [19][20]. Proteins were expressed in BL 21*E Coli* strands following induction with IPTG and purified by elution through Nickel affinity columns (GE Healthcare Bio-Sciences AB, Uppsala, Sweden). The His Tag was efficiently removed by cleavage with 45% formic acid at 45ºC for 5 h, following exhaustive dialysis against buffer Tris 20 mM, NaCl 150 mM, pH 8.0). A second metal affinity chromatography step was run to separate the final pure protein fraction.

Mass Spectrometry Analysis

Protein digestion and Mass Spectrometry analysis were performed at the Proteomics Core Facility CEQUIBIEM, at the University of Buenos Aires/CONICET (National Research Council) as follows: Protein samples were reduced with dithiothreitol (DTT) and alkylated with iodoacetamide in Ammonium Bicarbonate 50 mM pH 8.0. This protein solution was precipitated with trichloroacetic acid (TCA). Proteins were resuspended in the same buffer, digested with trypsin (Promega V5111), peptides purified and desalted with ZipTip C18 columns (Millipore). The digests were analyzed by nanoLC-MS/MS in a Thermo Scientific Q-Exactive Mass Spectrometer coupled to a nanoHPLC EASY-nLC 1000 (Thermo Scientific). For the LC-MS/MS analysis, approximately 1 µg of peptides was loaded onto a reverse phase column (C18, 2 µm, 100 A, 50 µm x 150 mm) Easy-Spray Column PepMap RSLC (P/N ES801) suitable for separating protein complexes with a high degree of resolution. The MS equipment has a high collision dissociation cell (HCD) for fragmentation and an Orbitrapanalyzer (Thermo Scientific, Q-Exactive). XCalibur 3.0.63 (Thermo Scientific) software was used for data acquisition and equipment configuration that allows peptide identification at the same time of their chromatographic separation. Full-scan mass

spectra were acquired in the Orbitrap analyzer. Q-Exactive raw data were processed using Proteome Discoverer software (version 2.1.1.21 Thermo Scientific) and searched against apoA-I sequence database downloaded from NCBI (National Center for Biotechnology Information) (www.ncbi.nlm.nih.gov) digested with trypsin with a maximum of one missed cleavage per peptide.

The exponentially modified protein abundance index (emPAI) was calculated automatically by Proteome Discoverer software and used to estimate the relative abundance of identified proteins within the sample.

Protein structure and chemical stability

ApoA-I Wt, W50R and L60R were diluted in Tris 20 mM pH 7.4 (Tris buffer) or citrate phosphate McIlvaine's buffer(Citrate buffer) pH 5.0 [21]. Variants were taken at 0.2 mg/mL (at 25°C). Tryptophan (Trp) intrinsic fluorescence emission spectra was acquired in an SLM4800 spectrofluorometer (ISS Inc, Champaign, IL) upgraded by Olis, setting the excitation wavelength at 295 nm and scanning emission from 310 to 400 nm. Solvent exposure of Trp residues was determined as a parameter of protein structural arrangement. ApoA-I variants were diluted to 0.1 mg/mL (in Tris buffer). Quenching of the Trp residues was determined by measuring intrinsic fluorescence following stepwise addition of acrylamide from a concentrated stock solution. The quenching constant K was calculated from a linear plot of the Stern-Volmer equation as:

$$F_0/\Delta F = 1/(fa \times K\,[Q]) + 1/fa \quad (1)$$

where fa is the fraction of the initial fluorescence which is accessible to the quencher, K is the Stern-Volmer quenching constant of the accessible fraction and [Q] is the

concentration of the quencher. F_0 is the initial fluorescence in the absence of quencher and ΔF is the remaining fluorescence after the addition of acrylamide at each concentration [22][15].

In order to sense hydrophobic pockets within the proteins spatial arrangements, the binding of Bis-ANS was measured following titration of the probe to apoA-I variants. Proteins were set at 0.1 mg/mL in Tris buffer and Bis-ANS added in small amounts from a methanol stock. Both, total intensity and spectral shift were registered by excitation at 395 nm and emission scanned from 450 to 550 nm [15]. Circular dichroism (CD) measurements were acquired on a Jasco J-810 spectropolarimeter. To register far UV spectra (200–290 nm), proteins were diluted in phosphate 10 mM buffer, pH 7.4 to 0.2 mg/mL in a 1 mm path-length cuvette, and three scans at a speed of 20 nm min^{-1} were registered and averaged to minimize noise signal. Mean residue weight values of 115.5, 115.4 and 115.7 for Wt, were estimated to calculate molar ellipticity as previously described [23]. Near CD spectra were registered under the same conditions but with a final protein concentration of 1.0, 1.5 and 1.5 mg/mL for Wt, W50R, and L60R, respectively.

To characterize apoA-I variants` stability respect to the Wt, Trp fluorescence spectra were measured following stepwise additions of increasing amounts of GdmCl [15][14]. As described in our previous works, the free energy of unfolding in the absence of denaturant (ΔG°H2O) was calculated from the shift of the Trp spectral center of mass as a function of GdmCl final concentration assuming the simplest two state process model [18][19].

In order to compare the self-association of the proteins in solution, Wt, W50R, and L60R were taken to 0.5 mg/mL in Phosphate Buffer (pH 7.4) and eluted through a Sepharose 200 HR column (Amersham Pharmacia recommended MW 10,000-600,000),

189 at a Flow rate of 0.35 mL/min, connected to a Merck Hitachi Fast Performance Liquid
190 Chromatography equipment. Elution profile was followed by UV detector (280 nm).
191

192 ## Partial degradation by proteolysis

193 In order to compare the accessibility of the variants to partial proteolysis,
194 proteins were incubated at 37°C in Tris buffer with Trypsin at a molar ratio apoA-I
195 variants to enzyme 1000:1. At different periods samples were heated in boiling water,
196 resolved by SDS PAGE, and developed by silver staining. The associated intensity of
197 the protein remaining within the monomer molecular weight was quantified with the
198 Image J 1.51 j8 Software. In the same trend, proteins were incubated with
199 metalloproteinase 12 (molar ratio protein to enzyme 500:1) and analyzed in the same
200 way.
201

202 ## Detection of protein aggregates

203 Thioflavin T (ThT) is widely used to detect amyloid-like structures [24].
204 Although ThT-associated quantum yield usually increases proportionally to the
205 formation of fibrillar protein aggregates, significant fluorescence is detected even when
206 proteins are present as oligomeric conformations [25][26]. To address the effect of pH
207 on the yield of amyloid-like protein aggregates, Wt (0.2 mg/mL) was taken for 48 h at
208 37°C at different pH between 7.4 and 5.0 in Citrate phosphate buffer, and ThT added at
209 a molar ratio of two with respect to protein. Associated fluorescence intensity was
210 measured on a Beckman Coulter DTX 880 Microplate Reader (Beckman, CA) through
211 the excitation (430 nm) and emission (480 nm) filters. The relative size of the
212 aggregates was estimated by light scattering on theSLM4800 spectrofluorometer
213 measuring light intensity at 90° with excitation and emission wavelength set at 400 nm.

Next, to compare the efficiency of the variants to bind to heparin, 0.2 mg/mL of Wt, W50R, and L60R, were incubated for 48 h at 37°C, pH 5.0. Both fluorescence and scattering were determined in the Microplate Reader, in the latter case by fixing excitation and emission filters at 350 nm.

To characterize nanometer-scaled aggregates conformations, Transmission electron microscopy (TEM), was performed on a JEOL-1200 EX. Negative staining is widely used to increase the contrast as the stain surrounds the sample but is excluded from the occupied volume and is thus observed as 'negative stain' [27]. Samples incubated at 0.6 mg/mL (37°C for 7 days) were seeded on Formvard grids, 0.5% phosphotungstic acid was added and visualized by negative staining. Magnification was 100,000 x.

Lipid interaction properties of apoA-I variants

Sodium dodecyl sulfate (SDS) is a negative lipid which mimics some characteristics of biological membranes [28]; in addition, it has been described to elicit the formation of fibrils from different peptides and proteins if used below the critical micellar concentration (CMC). We have previously shown that Wt binds to this lipid increasing ThT fluorescence [15]. To analyze the comparative binding of SDS to apoA-I variants, proteins were incubated in citrate phosphate buffer pH 7.4 for 48 h at 37°C in the presence or absence of 0.2 mM SDS. Previously we have confirmed that under those conditions SDS is far lower from the CMC. ThT-associated fluorescence and scattering were measured as described above.

DMPC clearance assay was used to give account for apoA-I function in lipid solubilization. As proteins are incubated with this phospholipid at its transition

239 temperature the decrease in turbidity indicates the efficiency to form lipid-protein
240 complexes. DMPC was solubilized in chloroform and desired amounts were dried under
241 extensive N_2 flow and additional vacuum. Lipids were resuspended in Tris buffer and
242 Multilamellar liposomes (MLV) were obtained by exhaustive vortexing. Lipid clearance
243 was determined by incubating proteins with DMPC MLV at a molar ratio lipid:protein
244 40:1 at 24°C for 90 min and absorbance monitored on the Microplate Reader by setting
245 filters at 350 nm [15].
246

247 ## Pro-inflammatory response induced by variants

248 In order to determine whether a soluble conformation of W50R and L60R could
249 elicit cellular pro-inflammatory pathways, the human-derived THP-1 Cell Line (from
250 Leukemic monocytes, ECACC, Salisbury, UK) was seeded (10^6 cells/mL) in RPMI
251 1640 medium in the presence of 10% fetal bovine serum (FBS), 100 U/mL Penicillin,
252 and 100 ug/mL Streptomycin at 37°C in a humidified incubator containing 5% CO_2.
253 Monocytes were activated by the addition of 5 ng/mL of Phorbol esters for 48 h [29].
254 Transformation into macrophages was observed by cellular adhesion to the plate.
255 Thereafter, medium was removed and apoA-I variants (at 1.0 µg/mL) added to the cells
256 and incubated for3 h in RPMI medium plus 0.5% FBS, in the presence of the same
257 antibiotic mixture and Polymyxin B (final concentration 50 µg/mL). Positive and
258 negative controls were determined by addition of 50ng/mL of bacterial lipo
259 polysaccharide (LPS) in the absence of the presence of Polymyxin B, respectively. Cells
260 were spun at 2,100 rpm for10 min to remove cellular debris, supernatant separated and
261 tumor necrosis factor α (TNF-α) and interleukin-1β (IL-1β) release were compared by
262 specific enzyme immunoassay from BD Biosciences (San Diego, CA) used according to
263 the manufacturer's instructions. Cell viability under these incubation conditions was

264 checked by the 3-(4,5-dimethylthiazolyl)-2,5-diphenyl-tetrazoliumbromide (MTT) cell
265 viability assay as previously described [14].
266

267 ## Other analytical methods

268 Protein content was quantified by the Bradford technique [30] or by absorbance
269 from the estimation of the extinction coefficient (32,430 $M^{-1}cm^{-1}$at 280 nm) as
270 determined in a Bio-Rad spectrophotometer (Hercules, CA).Unless otherwise stated, the
271 results were reproduced in three independent experiments and are indicated as means ±
272 standard error. Statistically significant differences between experimental conditions
273 were evaluated by the Student´s test.
274

275 # Results

276 ### Structural comparison and stability

277 The expression and isolation procedures used in this study yielded high amounts
278 of pure proteins. We have previously shown that the lack of the two first amino acids
279 resulting from the acidic cleavage does not introduce modifications in protein function
280 or structure with respect to the plasma apoA-I [20]. In order to confirm the chemical
281 integrity and purity, the Wt variant was subjected to LC-MS/MS equipped with an
282 Orbitrap analyzer. Exponentially Modified Protein Abundance Index (emPAI) estimated
283 an abundance of 99.95 for this protein. Previous to each experiment, in order to ensure a
284 fresh folding, proteins were solubilized in GdmCl 2 M and extensively dialyzed through
285 the desired buffer.
286

Due to the location in the primary structure of the four Trp residues in apoA-I molecule (8, 50, 72 and 108), the average intrinsic fluorescence is representative of the conformation of the N-terminal domain (residues 1-184) [31]. In order to compare proteins structure, we prepared freshly refolded apoA-I variants and characterized Trp fluorescence spectra. While the wavelength of maximum fluorescence (WMF) of W50R was similar to the Wt, a small but significant red shift (4 nm +/-1) was observed for L60R (Table 1).

Table 1 Spectral characterization of N terminal apoA-I variants.

	WMF[a] pH 7.4 (nm)	**Relative intensity[b]**	**K [c]**	**AG°(H_2O) [d] (kcal/mol)**	**WMF [a] pH 5.0 (nm)**
WT	338 +/- 1	5.5 +/- 0.3	5.6 +/- 0.3	2.3 +/- 0.1	339 +/- 2
W50R	340 +/- 2	3.8 +/- 0.5	8.6 +/- 0.4	1.7 +/- 0.1	340 +/- 2
L60R	342 +/- 2 **	3.6 +/- 0.5	8.3 +/- 0.4	ND	342 +/- 2

[a] Wavelength of maximum fluorescence ** denotes difference with respect to Wt at P<0.01.

[b] Fluorescence Intensity at the WMF, with all the proteins at 0.1 mg/mL and under exactly the same slit and high voltage gain

[c] Stern-Volmer quenching constant for the quenching of 4 Trp residues by Acrylamide

[d] Free energy change of unfolding from equilibrium unfolding curves as shown in Fig 1.

Both mutants showed lower intensity than the Wt for identical protein concentration. A significantly higher Stern-Volmer constant (K) calculated from the analysis of Trp quenching with acrylamide (8.6+/- 0.4 for W50R and 8.3+/- 0.4 for L60R) indicates a higher exposure of the Trp environments to solvent in both mutants as compared to the Wt form (K 5.6 +/- 0.3).

To better estimate apoA-I natural variants` conformational stability, fluorescence was followed after titration with GdmCl. The chemical denaturation pattern obtained from the shift in the center of mass of the Trp emission has been extensively used to give account for the protein stability under chaotropic solvents [32]. As previously discussed, this parameter is in good agreement with the measurement of the emission intensity at a fixed wavelength at increasing GdmCl concentration, and better help to compare our previous data [14][15]. While the free energy of denaturation ($\Delta G^{\circ}H_2O$) for W50R (1.7 kcal/mol) is lower than the value estimated for the Wt (2.3 kcal/mol), the dependence fit of Trp emission with GdmCl is far from a two state (native and unfolded) model for L60R (Fig 1A), and thus we were not able to precisely calculate this parameter. Interestingly, its total intrinsic fluorescence intensity is lower than the one of the Wt, even though it keeps the four native Trp residues. As long as protein is unfolded by titration with GmdCl the total intensity tends to equal that of the Wt (Inset Fig 1A).

Fig 1. Structural characterization of apoA-I variants. Chemical equilibrium unfolding of apoA-I in Tris 20 mM buffer pH 7.4 (A) and pH 5.0 in Citrate phosphate

326 buffer (B) was evaluated at a starting protein concentration of 0.2 mg/mL; Trp
327 fluorescence was registered with excitation at 295 nm and emission between 310 and
328 400 nm; spectral center of mass was plotted as a function of [GmdCl]. Circles, squares
329 and triangles represent Wt, W50R, and L60R, respectively. Lines correspond to fittings
330 of a sigmoideal model to the data. Y-left axe corresponds to Wt and W50R, and Y-right
331 axe to L60R. Inset Fig A represents the dependence of the total intensity of L60R
332 respect of Wt as a function of [GmdCl]. Circular dichroism in the far (C) or near (D)
333 UV region are represented for Wt (dark), W50R (dark grey) and L60R (clear grey).
334
335
336 In order to test whether a local decrease in pH could induce a disruption in
337 protein structure, variants were taken to pH 5.0 and denaturation curves repeated under
338 the same conditions. As Fig 1B shows, the behavior remains similar to that obtained
339 under physiological pH, indicating a mild effect of an acidic milieu on proteins`
340 conformation.

341 CD analysis of protein structure in the far UV reveals a conserved α helical
342 secondary structure which was previously identified for the Wt protein at low
343 concentrations (Fig 1C) [33]. The secondary structure content was calculated with the
344 algorithm CONTIN rendering a high percentage of helical structure for all the three
345 proteins [34]. The Wt spectrum is almost indistinguishable from that of W50R and
346 slightly more intense than that of L60R. Accordingly, a loss of about 4 and 7% of alpha
347 helical structure is observed for the W50R and L60R variants, respectively.

348 The comparison among the tertiary structures was analyzed by CD in the near
349 UV (Fig 1D); spectra of both mutants preserve fine structure although the lower

intensity from 280 nm to 250 nm indicates mild structural differences among the aromatic amino acid residues.

Partial proteolysis sensitivity is usually evaluated in order to give information about the accessibility of protein domains within the spatial arrangement. Thus, variants were incubated at increasing times with either trypsin or metalloproteinase 12 (MMP12), and run through an SDS PAGE visualized with Silver staining; the time dependent efficiency of the proteolysis could be observed and quantified by the disappearance of the band corresponding to the original Molecular weight (Fig 2A). The digestion rate of the major fragment is higher as long as the incubation time increases indicating the efficiency of the proteolysis.

Fig 2. Partial proteolysis of apoA-I variants. Proteins were incubated at 0.3 mg/mL in Tris 20 mM buffer pH 7.4 with trypsin or MMP12 at molar ratios of 1000:1 or 500:1apoA-I variants to enzyme respectively. After different time periods, reactions were stopped by the addition of sample running buffer and two minutes boiling. Samples were run through a SDS PAGE (16%) and developed by silver staining. A) Black/white representation of the initial (0) and final (60 min) incubation times. Intensity remaining with the monomeric molecular weight (28 kDa) after B) Trypsin or C) MMP12 treatments was quantified by the Image Quant software and normalized to the intensity of the band at time= 0 for each protein. Circles, squares and triangles correspond to Wt, W50R and L60R respectively (** represents $P< 0.001$ with respect to the same time in the Wt).

After 45 minutes incubation under these conditions and in agreement with Das et al [16] the proteolysis of W50R showed a similar yield as the Wt, instead it demonstrated to be significantly more efficient for L60R with both enzymes tested.

The extrinsic fluorescence probe ANS (or its dimer Bis-ANS) was extensively used to test the spatial arrangements of proteins, due to the fact that is it weakly fluorescent in water but its quantum yield increases significantly, and its emission shifts upon binding to proteins. Its emission is proposed to sense specifically protein hydrophobic pockets and "molten globule" like states [32]. We and others have previously shown that binding of Bis-ANS to apoA-I Wt is efficient and fast [14][15]. We herein show (Fig 3), as it was previously demonstrated with the monomer ANS, that W50R binds Bis-ANS with a relatively higher quantum yield than the Wt [17].

Fig 3. Binding of Bis-ANS to apoA-I variants Proteins were diluted at a final concentration of 0.1 mg/mL (Tris 20 mM pH 7.4 buffer) and titrated with small amounts of Bis-ANS to a final concentration of 16 μM. Fluorescence was detected in the SLM 4800 spectrofluorometer setting excitation at 360 nm, and intensity of the emission registered at the observed Wavelength of Maximum Fluorescence (WMF) for the probe (490 nm). As in Fig. 1 circles, squares and triangles represent Wt, W50R, and L60R, respectively. Inset: spectra of Bis-ANS at a molar ratio 4:1 probe to protein normalized at the WMF. Continuous and dashed lines represent Wt and L60R respectively.

Instead, intensity of the Bis-ANS associated to L60R is lower indicating a lower permeation or binding of this probe within the spatial protein arrangement. Nevertheless, WMF of the Bis-ANS bound to L60R is similar to the probe associated to the Wt (Fig 3 inset). In a different experiment, to evaluate whether the presence of the hydrophilic group in the mutants may disrupt the protein self-association, freshly folded Wt and variants were run under FLPC; the elution pattern demonstrated that most of the Wt migrates as a dimer with a minor fraction (about 20%) eluting as a monomer (S. Fig 1). This pattern is well preserved for both mutants.

Aggregation tendency

The variants tendency to aggregate under physiological pH and low concentrations was evaluated by incubating proteins at 0.2 mg/mL for 48 h in Citrate buffer pH 7.4. The ThT measurement indicates as previously observed for the Wt that amyloid complexes were not detected under these conditions (dark gray bars in S. Fig 2). In a parallel experiment, proteins were further incubated at 0.6 mg/mL for 7 days under the same conditions and observed by Transmission Electron Microscopy (Fig 4).

Fig 4. Observation of apoA-I mutants' aggregates at physiological pH. Wt (A), W50R (B) or L60R (C) were incubated for 7 days at 0.6 mg/mL and 37 ºC in Citrate phosphate buffer pH 7.4. Aggregates were observed by negative staining under Transmission Electron Microscopy on a JEOL-1200 EX Microscope. Bars in each image show the scale used.

The sample of the Wt showed a low degree of amorphous-like aggregates and small amounts of protofibers (Fig 4A). Both mutants (W50R and L60R, Fig 4B and C respectively) were represented by a higher yield of aggregates with similar morphology. In addition protofibers of about 8-10 nm diameter are observed under these conditions. The behavior of these proteins was similar to other mutants analyzed under the same conditions [14][15].

Binding to ligands

Heparin is usually used as a model of glycosamino glycans (GAGs), which are supposed to play key roles in the maintenance of cellular functions. Moreover, it is proposed that interactions of proteins with GAGs could result in the retention or aggregation of proteins inducing amyloidosis [35][36], but instead they could compete avoiding cellular toxicity or conformational shifts [37]. Within this frame in mind, we analyzed binding of both natural mutants to heparin either at physiological pH or under acidic conditions. ThT results suggest, as observed before for the Wt under these conditions [19], that the presence of heparin does not induce a significant structural arrangement of the variants when incubated at pH 7.4 for 2 days at 37ºC (clear gray bars

449 in S Fig 2). As long as pH decreases, protonation of His residues may result in the gain
450 of positive charges of the proteins thus helping electrostatic interactions with the
451 negative groups of the GAGs. As the isoelectric point of apoA-I is estimated in 5.27, we
452 analyzed the effect of an acidic environment on apoA-I aggregation and interaction with
453 heparin by incubating Wt at different pH between 5.0 and 7.4, in the absence or the
454 presence of this model of GAG. Size and amyloid-like tendency of the complexes were
455 followed by scattering (Fig 5A) and ThT fluorescence (Fig 5B). These data indicate that
456 the formation of Wt amyloid-like complexes is favored as long as pH decreases (dark
457 gray bars), and this tendency is increased in the presence of heparin (clear gray bars).
458

459 **Fig 5. Influence of acidic pH on heparin binding.** A and B) Wt was solubilized at 0.2
460 mg/mL at different pH from 7.4 to 5.0 by using Citrate phosphate buffer and incubated
461 either in the absence (dark gray bars) or the presence (clear gray bars) of heparin at a
462 molar ratio 1:1 protein to GAG for 48 h at 37ºC. A) Light scattering at 90ºwas
463 determined in the spectrofluorometer with excitation and emission wavelengths at 400
464 nm; B) ThT associated fluorescence was determined in the Multiplate Reader with
465 excitation set at 430 and emission filter at 480 nm. Bars correspond to mean ± SD.
466 Differences were analyzed by ANOVA followed by Tukey test. Different letters
467 symbolize significant differences ($P<0.05$). C and D) Wt, W50R, and L60R, were taken
468 at pH 5.0 in Citrate phosphate buffer (0.2 mg/mL) and incubated in the absence (dark
469 gray bars) or the presence (clear gray bars) of heparin at a molar ratio of 2 per mol of
470 protein at 37ºC by 48 h. C) Scattering was analyzed in the Microplate Reader with filter
471 set a 340 nm; D) ThT associated fluorescence was quantified as described in Fig 5B.
472 Symbol ** in C and D corresponds to differences with $P<0.001$ with respect to Wt
473 under the same conditions.

Next, we compared the binding of the variants under study to this model of GAG at pH 5.0. As shown, a higher scattering (Fig 5C) and ThT associated fluorescence (Fig 5D) in the case of W50R indicates its higher efficiency to bind to heparin as amyloid-like complexes under acid conditions while L60R behaves similar to Wt.

In order to answer whether the structural disruption induced by a change in the amino acid sequence (and charge) of the apoA-I variants could modify their interactions with negative ligands in the microenvironment, we incubated W50R and L60R with SDS, which not only is a good model of membrane lipids but also was suggested to work as inductor of amyloid-like complexes formation from different proteins when incubated under the lipid critical micellar concentration (CMC: 0.7 mM) [38]. Fig 6 shows, as previously observed, a strong increase in ThT fluorescence of Wt protein when bound to SDS [15] which is in a similar trend for W50R and with a higher yield for L60R.

Fig 6. Protein binding to SDS. ApoA-I were incubated at a concentration of 0.2 mg/mL in Citrate phosphate buffer pH 7.4 in the absence (dark gray bars) or in the presence (clear gray bars) of 0.2 mM SDS. After 48 h at 37°C ThT was added to a 1:1 molar ratio to protein and relative fluorescence quantified as described in Figure 5D. The symbol * denotes difference with respect to Wt at $P<0.05$.

Effect of mutations on lipid clearance and cellular responses

It is clear that the conformational flexibility could alter the equilibrium between function and toxicity, and thus we set out to test whether the structural shift detected in the N terminus of L60R could affect the protein interaction with a model of membrane. It is well known that the analysis of MLV clearance at the lipid transition temperature is a traditional functional parameter to test efficiency of apoA-I for lipids solubilization. Fig 7 shows that the L60R mutant clears DMPC MLV with a small by significantly higher efficiency than the Wt indicating a conserved function in lipid binding.

Fig 7. Characterization of the mutant L60R on the spontaneous formation of lipid:protein complexes. Multilamellar DMPC liposomes were incubated at 24°C in the presence of Wt (circles) or L60R (triangles) at a 80:1 lipid to protein molar ratio. Absorbance was measured at 340 nm in the Microplate Reader. Significant difference among both variants was determined by comparing absorbance at the last point of the measured kinetics (120 min). L60R Absorbance was different with respect to Wt at $P<0.05$ as measured by the Student´s Test.

Finally, and in order to test the hypothesis that apoA-I variants could induce cellular responses associated to a pro-inflammatory landscape, we compared the release of TNF-α and IL-1β from THP-1 cells, which is widely used as a human model of macrophages. As Fig 8A and B show, while W50R behaves as the Wt, L60R induced the release of these cytokines. MTT reduction measurements indicated that cell viability was preserved under the different conditions tested (not shown)

Fig 8. Induction of TNF-α (A) and IL-1β (B) release from cultured macrophages. THP-1 human monocytes were activated to macrophages by the addition of 5 ng/mL of Phorbol esters for 48 h. One μg/mL (A) or 0.5 μg/mL (B) of Wt, W50 or L60R were incubated with the cells for 3 h in the presence of Polymyxin B. Incubation of cells with LPS, either in the presence (LPS +P) or absence (LPS -P) of Polymyxin B, was used as negative and positive control respectively. P represents an extra negative control in which cells are incubated only in the presence of Polymyxin B. Symbol #represents significant difference respect to negative control (LPS +P) at $P< 0.05$. Symbol ** represents significant difference with respect to Wt at $P< 0.001$.

Discussion

Structural flexibility is essential for apolipoproteins in order to fulfill complex functions, as it is required for apoA-I to interact within micro environmental ligands to solubilize lipids; nevertheless, this property may put the proteins into the risk of suffering subtle structural shifts from the native structure. The late-onset of the clinical manifestations of the amyloidosis disease due to apoA-I variants supports the fact that the final fibrillar conformation detected in the lesions is probably the result of progressive events that cooperate to give rise to the insoluble protein aggregates. Thus, it could be possible that a higher yield of partially folded variants could work late as seeding events in the long term period.

The structural modifications that result from the natural mutations in apoA-I are

549 not easily predicted. Interestingly, although G26R, W50R, and L60R experiment a
550 similar substitution in the N terminus (the replacement of a neutral amino acid by an
551 Arg), only little disorder is observed for G26R [16] and W50R (this work and others
552 ([16]; instead the structural arrangement observed herein for L60R is more evident. Das
553 et al suggested that more than a strong conformational shift, the mutations in apoA-I
554 may induce perturbations, increasing the accessibility of amyloid-prone segments that
555 favor protein aggregation [16]. Such mild perturbations could increase the cleft from the
556 α helical bundles allowing the accessibility to not-yet-described proteases which help
557 the release of the peptides identified in the lesions. By an elegant model, they propose
558 that desestabilization of the four-helix bundle containing residues may favor the
559 formation of a resistant amyloid core by interactions of the N-terminal amyloid hot
560 spots.

561 In agreement with Das et al. [16], our fluorescence and dichroism spectroscopic
562 measurements (a small red shift in the Trp environment and a preserved secondary
563 structure) suggest a mild effect of the Trp substitution by an Arg in position
564 50.Mutation W50R is comprised in the middle of the segment L44−S55 which was
565 shown in the crystal structure having an extended conformation consistent with the β-
566 strand-like geometry (Fig 9). It was proposed that the exposure of this segment could
567 initiate the α-helix to β-sheet apoA-I conversion in amyloidosis. Nevertheless, the
568 disruptive presence of a positive charge in replacement of the aromatic Trp is detected
569 in our experimental design by an increased yield in the Bis-ANS binding and minor
570 change in the near UV spectra, together with the detection of stronger binding to
571 heparin at acidic pH. It is worth mentioning that the N-terminal 1–83 fragment of W50R
572 variant was shown to participate in heparin-mediated fibril formation [39].
573

574

575 **Fig 9: Locations of amyloidogenic mutations W50R and L60R in the structure of**
576 **apoA-I.** The structure was obtained by the PyMOL Molecular Graphics System,
577 Version 2.0 (Schrödinger, LLC), from the X-ray crystal structure of Δ(185−243) apoA-I
578 (PDB ID 3R2P). N terminal residues subjected to mutations are shown in stick
579 representation.

580

581 Acidic intracellular milieu was associated to macrophages activation within
582 inflammatory lesions [40]. As mentioned above, the W50R variant is one of the few
583 exceptions in which apoA-I mutants' deposits are associated to the glomeruli [13][41].
584 The extracellular matrix (ECM), especially the proteoglycans (PGs) have diverse
585 biologic functions, including binding of growth factors and regulation of collagen
586 fibrillogenesis [42], and their composition is tissue specific [43]. In addition, it was
587 found that decorin (a dermatan/chondroitin sulfate PG) accumulated in amyloid
588 deposits, but not in deposits of fibrillary glomerulo nephritis [44]. From our previous
589 studies we learnt that binding of proteins to GAGs seems to be a cooperative, specific
590 interaction [45]. We have previously observed that the amyloidogenic mutant R173P
591 shows sensitive binding to heparin under physiological pH in spite of the loss in one
592 positive charge, probably due to the exposition of cryptic positive residues which are
593 accessible by the break in the amphipatic helix induced by the Proline residue in
594 position 173 [15]. Even though binding at physiologic pH is not clear for the mutants
595 tested here it is expected that the acidic milieu may strength protein-GAGs interactions.
596 Although further studies are worth to be done, it could be speculated that the positive
597 Arg charge could induce a stronger retention within the glomeruli`s GAGs thus helping

598 its aggregation, especially under situations of kidney disease associated to
599 inflammation.

600 As mentioned above, L60R shows (as compared to Wt), a red shift in Trp
601 fluorescence which may indicate a relatively higher exposure of these aromatic residues
602 to the polar environment. Due to the average contribution of the 4 Trp in the native
603 structure, this shift may indicate either a subtle movement of side chains or larger scale
604 conformational changes of the protein. The observed lower binding to Bis-ANS may
605 suggest that the disruption of the bottom hydrophobic cluster by the positive charge of
606 the Arg (Fig 9) could bring this amino acid more exposed, as it results from a higher
607 binding to SDS which is not detected for the other amyloidogenic mutant tested in this
608 work (Fig 6); moreover, this structural disorder should allow the permeation of
609 proteases, as it is shown here. Although trypsin is not a physiological protease of apoA-
610 I in circulation, it helps to get insight into protein structure. In order to compare trypsin
611 induced proteolysis, we analyzed by the expassy software (www.expasy.org) the
612 predicted sites to be substrate of this enzyme. Arg in position 60 should separate only
613 one amino acid from a predicted fragment of three residues (59-61). Nevertheless, a
614 higher efficiency of this variant´s processing is observed (Fig 2); the same tendency is
615 detected under this experimental design by using MMP-12. Altogether, the
616 rearrangement of the Trp environment in the L60R mutant, the higher accessibility to
617 proteases and the lower CD spectral signal at 255-280 nm respect to the Wt agree with a
618 spatial rearrangement with a decreased stability and an increase in protein flexibility.
619 The increased susceptibility to proteases could explain the appearance of a 10 kDa
620 molecular mass N terminal peptide within the lesions [8], although interestingly *in vitro*
621 studies with the 93-residue N-terminal fragment demonstrated that the peptide freed

622 behaves similar to Wt in the aggregation pattern than the same peptide with the Wt
623 sequence [46].

624 In addition to protein misfolding, it is worth to consider the possibility that at
625 least part of the clinical manifestations could be due to a loss in protein function, such
626 as lipid binding, which in addition could increase the amount of lipid-free protein,
627 amyloid-prone precursors. In order to consider this possibility, we first modeled the
628 domain in which the mutation occurs (amino acids 52-65) in a helix wheel modeling
629 software (http://lbqp.unb.br/NetWheels/). The modeling predicts that due to the
630 periodicity that brings in close proximity residues Val53, Leu64 and Phe57, the Leu 60
631 contributes to form the apolar phase of the putative amphipatic class A α-helix (Fig10).
632
633
634 **Fig 10. Helical wheel model of the putative α-helix comprising residues 52-65 of**
635 **apoA-I** Wt sequence represented as an helix seen down the long axis, with an amino
636 acid arrangement considering an ideal α-helix (l00^{o} rotation per amino acid). Gray scale
637 in the Figure corresponds to the nature of different amino acids. Toward the right side
638 of the helix it is indicated the replacement of Arg in position 60 in the nonpolar phase.
639
640
641 The positive charge of the Arg may thus perturb the hydrophobic bottom cluster.
642 The mutation in position 60 should in addition disrupt a Leu zipper stabilized with other
643 Leu residues in the same molecule or with a second molecule in the native dimer [47].
644 In our hands the shift among dimer and monomer conformation was not dramatically
645 modified (S. Fig 1). Moreover, this effect is not drastic enough to decrease the
646 efficiency to solubilize neutral lipids (Fig 7) as it is the case with W50R and G26R

647 substitutions [16]. Instead, it could be that the relative exposition of the positive charge
648 in this segment could favor its interactions and/or shift toward a pathological amyloid-
649 like structure when interacting with other ligands, as negative lipids, as it suggested by
650 the SDS binding experiments.

651 Finally, we have recently shown that other N terminal apoA-I mutant
652 (Gly26Arg), induces the release of TNF-α and IL-1β from a model of macrophages
653 [14], in a pathway probably involving the specific activation of the NF-κB pro-
654 inflammatory cascade [48]. The kidney is a major target organ of innate immune
655 inflammatory diseases. The deposition of the acute-phase reactant serum amyloid A
656 (SAA) as amyloid causes progressive glomerular and vascular damage and leads to
657 organ failure [49]. It was suggested that this and other misfolded proteins could be
658 recognized by pattern recognition receptors (PRRs) resulting in the activation of pro
659 inflammatory cascades, being increased IL-1β secretion responsible for most of the
660 systemic features of this group of disorders [50]. IL-1β production may induce the
661 synthesis of other cytokines as TNF-α. Our results shown here indicate that mild
662 conformational rearrangement detected for L60R variant may induce the activation of
663 the microenvironment toward a pro-inflammatory landscape which could help to
664 perpetuate events triggering organ damage.

665 In conclusion, in agreement with other groups, our data support that it is not
666 required a large overall destabilization of the tertiary structure of apoA-I to become
667 amyloidogenic; either reduced protection of the major amyloid “hot spot”, increased
668 susceptibilities to proteases or partial oxidation could induce cooperative shift toward a
669 misfolded conformation. Nevertheless, the chronic clinical phenotype indicates that the
670 landscape in which protein circulates (molecular crowding, acidification, oxidation,
671 interactions with ligands etc) could play key roles to give rise to amyloid species. These

672 species could either be nucleus of aggregation or, as we have previously suggested,
673 work as signal receptors starting up cellular events associated to the pathology. Further
674 research will help to explore different pathways.
675

676 Acknowledgements

677

678 Authors acknowledge Mr. Mario Ramos for invaluable help with Figures'
679 design. We include acknowledgements to Mrs Rosana del Cid for English assistance,
680 Lic Letizia Bauzá for FPLC measurements, to Lic Tomás Masson for help with Mass
681 Spec analysis and Miss Ana L. Rodriguez for technical assistance.
682
683

684 **References**

685 1. Schaefer EJ, Anthanont P, Asztalos BF. High-density lipoprotein metabolism,
686 composition, function, and deficiency. Curr Opin Lipidol. England; 2014;25:
687 194–199. doi:10.1097/MOL.0000000000000074
688 2. Wu BJ, Ong KL, Shrestha S, Chen K, Tabet F, Barter PJ, et al. Inhibition of
689 arthritis in the lewis rat by apolipoprotein A-I and reconstituted high-density
690 lipoproteins. Arterioscler Thromb Vasc Biol. 2014;34: 543–551.
691 doi:10.1161/ATVBAHA.113.302832
692 3. Barter PJ, Nicholls S, Rye KA, Anantharamaiah GM, Navab M, Fogelman AM.
693 Antiinflammatory properties of HDL. Circ Res. 2004;95: 764–772.
694 doi:10.1161/01.RES.0000146094.59640.13
695 4. Assmann G, Schmitz G, Funke H, Von Eckardstein A. Apolipoprotein A-I and
696 HDL deficiency. Curr Opin Lipidol. 1990;1: 110–115. doi:10.1097/00041433-

199004000-00005

5. Sorci-Thomas MG, Thomas MJ. The effects of altered apolipoprotein A-I structure on plasma HDL concentration. Trends Cardiovasc Med. United States; 2002;12: 121–128.

6. Van Allen MW, Frohlich JA, Davis JR. Inherited predisposition to generalized amyloidosis. Clinical and pathological study of a family with neuropathy, nephropathy, and peptic ulcer. Neurology. United States; 1969;19: 10–25.

7. Booth DR, Tan SY, Booth SE, Hsuan JJ, Totty NF, Nguyen O, et al. A new apolipoprotein Al variant, Trp50Arg, causes hereditary amyloidosis. QJM. England; 1995;88: 695–702.

8. Soutar AK, Hawkins PN, Vigushin DM, Tennent GA, Booth SE, Hutton T, et al. Apolipoprotein AI mutation Arg-60 causes autosomal dominant amyloidosis. Proc Natl Acad Sci U S A. United States; 1992;89: 7389–7393.

9. Rowczenio D, Stensland M, de Souza GA, Strøm EH, Gilbertson JA, Taylor G, et al. Renal Amyloidosis Associated With 5 Novel Variants in the Fibrinogen A Alpha Chain Protein. Kidney Int Reports. 2017;2: 461–469. doi:10.1016/j.ekir.2016.11.005

10. Kidd J, Carl DE. Renal amyloidosis. Current Problems in Cancer. 2016. pp. 209–219. doi:10.1016/j.currproblcancer.2016.08.002

11. Gregorini G, Izzi C, Obici L, Tardanico R, Röcken C, Viola BF, et al. Renal apolipoprotein A-I amyloidosis: a rare and usually ignored cause of hereditary tubulointerstitial nephritis. J Am Soc Nephrol. 2005;16: 3680–6. doi:10.1681/ASN.2005040382

12. Gregorini G, Izzi C, Ravani P, Obici L, Dallera N, Del Barba A, et al. Tubulointerstitial nephritis is a dominant feature of hereditary apolipoprotein A-I

amyloidosis. Kidney Int. 2015;87: 1223–1229. doi:10.1038/ki.2014.389

13. Tougaard BG, Pedersen KV, Krag SR, Gilbertson J a, Rowczenio D, Gillmore JD, et al. A case report of hereditary apolipoprotein A-I amyloidosis associated with a novel APOA1 mutation and variable phenotype. Eur J Med Genet. 2016;59: 474–7. doi:10.1016/j.ejmg.2016.05.015

14. Ramella N a, Schinella GR, Ferreira ST, Prieto ED, Vela ME, Ríos JL, et al. Human apolipoprotein A-I natural variants: molecular mechanisms underlying amyloidogenic propensity. PLoS One. 2012;7: e43755. doi:10.1371/journal.pone.0043755

15. Rosú SA, Rimoldi OJ, Prieto ED, Curto LM, Delfino JM, Ramella NA, et al. Amyloidogenic propensity of a natural variant of human apolipoprotein A-I: Stability and interaction with ligands. PLoS One. 2015;10: 1–17. doi:10.1371/journal.pone.0124946

16. Das M, Mei X, Jayaraman S, Atkinson D, Gursky O. Amyloidogenic mutations in human apolipoprotein A-I are not necessarily destabilizing - a common mechanism of apolipoprotein A-I misfolding in familial amyloidosis and atherosclerosis. FEBS J. England; 2014;281: 2525–2542. doi:10.1111/febs.12809

17. Das M, Wilson CJ, Mei X, Wales TE, Engen JR, Gursky O. Structural Stability and Local Dynamics in Disease-Causing Mutants of Human Apolipoprotein A-I: What Makes the Protein Amyloidogenic? J Mol Biol. 2016;428: 449–462. doi:10.1016/j.jmb.2015.10.029

18. Tricerri MA, Behling Agree AK, Sanchez SA, Bronski J, Jonas A. Arrangement of apolipoprotein A-I in reconstituted high-density lipoprotein disks: an alternative model based on fluorescence resonance energy transfer experiments. Biochemistry. 2001;40: 5065–5074. doi:bi002815q [pii]

19. Ramella N a, Rimoldi OJ, Prieto ED, Schinella GR, Sanchez S a, Jaureguiberry MS, et al. Human apolipoprotein A-I-derived amyloid: its association with atherosclerosis. PLoS One. 2011;6: e22532. doi:10.1371/journal.pone.0022532

20. Prieto ED, Ramella N, Cuellar LA, Tricerri MA, Garda HA. Characterization of a human apolipoprotein a-I construct expressed in a bacterial system. Protein J. Netherlands; 2012;31: 681–688. doi:10.1007/s10930-012-9448-z

21. Gomori G. Preparation of Buffers for Use in Enzyme Studies (by G . Gomori). Enzyme. 2004. pp. 2–10. doi:10.1016/0076-6879(55)01020-3

22. Lakowicz JR. Principles of Fluorescence Spectroscopy. Springer New York; 2006.

23. Schmid FX. Spectral methods of characterizing protein conformation and conformational changes. Protein structure A practical approach. 1989. pp. 251–285.

24. LeVine H. Quantification of β-sheet amyloid fibril structures with thioflavin T. Methods Enzymol. 1999;309: 274–284. doi:10.1016/S0076-6879(99)09020-5

25. Lindgren M, Sörgjerd K, Hammarström P. Detection and characterization of aggregates, prefibrillar amyloidogenic oligomers, and protofibrils using fluorescence spectroscopy. Biophys J. 2005;88: 4200–4212. doi:10.1529/biophysj.104.049700

26. Wetzel R, Chemuru S, Misra P, Kodali R, Mukherjee S, Kar K. An aggregate weight-normalized thioflavin-t measurement scale for characterizing polymorphic amyloids and assembly intermediates. Methods in Molecular Biology. 2018. pp. 121–144. doi:10.1007/978-1-4939-7811-3_6

27. Ellis RA. Principles and techniques of electron microscopy: Biological applications, Volume 9. Cell. 1979;17: 235–236. doi:10.1016/0092-

772 8674(79)90312-X

773 28. Tulumello D V., Deber CM. SDS micelles as a membrane-mimetic environment
774 for transmembrane segments. Biochemistry. 2009;48: 12096–12103.
775 doi:10.1021/bi9013819

776 29. Park EK, Jung HS, Yang HI, Yoo MC, Kim C, Kim KS. Optimized THP-1
777 differentiation is required for the detection of responses to weak stimuli. Inflamm
778 Res. 2007;56: 45–50. doi:10.1007/s00011-007-6115-5

779 30. Bradford MM. A rapid and sensitive method for the quantitation of microgram
780 quantities utilizing the principle of …. Anal Biochem. 1976;72: 248–254.

781 31. Davidson WS, Arnvig-McGuire K, Kennedy A, Kosman J, Hazlett TL, Jonas A.
782 Structural organization of the N-terminal domain of apolipoprotein A-I: Studies
783 of tryptophan mutants. Biochemistry. 1999;38: 14387–14395.
784 doi:10.1021/bi991428h

785 32. Martins SM, Chapeaurouge A, Ferreira ST. Folding intermediates of the prion
786 protein stabilized by hydrostatic pressure and low temperature. J Biol Chem.
787 United States; 2003;278: 50449–50455. doi:10.1074/jbc.M307354200

788 33. Mei X, Atkinson D. Crystal Structure of C-terminal Truncated Apolipoprotein A-
789 I Reveals the Assembly of High Density Lipoprotein (HDL) by. 2011.
790 doi:10.1074/jbc.M111.260422

791 34. Sreerama N, Woody RW. Estimation of protein secondary structure from circular
792 dichroism spectra: Comparison of CONTIN, SELCON, and CDSSTR methods
793 with an expanded reference set. Anal Biochem. 2000;287: 252–260.
794 doi:10.1006/abio.2000.4880

795 35. Cohlberg JA, Li J, Uversky VN, Fink AL. Heparin and other glycosaminoglycans
796 stimulate the formation of amyloid fibrils from ??-synuclein in vitro.

797 Biochemistry. 2002;41: 1502–1511. doi:10.1021/bi011711s

798 36. Aguilera JJ, Zhang F, Beaudet JM, Linhardt RJ, Colón W. Divergent effect of
799 glycosaminoglycans on the in vitro aggregation of serum amyloid A. Biochimie.
800 Elsevier; 2014;104: 70–80.

801 37. Oberkersch R, Attorresi AI, Calabrese GC. Low-molecular-weight heparin
802 inhibition in classical complement activaton pathway during pregnancy. Thromb
803 Res. 2010;125. doi:10.1016/j.thromres.2009.11.030

804 38. Ahmad MF, Ramakrishna T, Raman B, Rao CM. Fibrillogenic and Non-
805 fibrillogenic Ensembles of SDS-bound Human α-Synuclein. J Mol Biol.
806 2006;364: 1061–1072. doi:10.1016/j.jmb.2006.09.085

807 39. Mikawa S, Mizuguchi C, Nishitsuji K, Baba T, Shigenaga A, Shimanouchi T, et
808 al. Heparin promotes fibril formation by the N-terminal fragment of
809 amyloidogenic apolipoprotein A-I. FEBS Lett. 2016;590: 3492–3500.
810 doi:10.1002/1873-3468.12426

811 40. Oorni K, Rajamaki K, Nguyen SD, Lahdesmaki K, Plihtari R, Lee-Rueckert M,
812 et al. Acidification of the intimal fluid: the perfect storm for atherogenesis. J
813 Lipid Res. 2015;56: 203–214. doi:10.1194/jlr.R050252

814 41. Samillán-sosa R, Sención-martínez G, Lopes-martín V, Martínez-gonzález MA,
815 Solé M, Luis J, et al. Amiloidosis renal hereditaria por depósito de
816 apolipoproteína AI : un reto diagnóstico. NEFROLOGíA. Sociedad Española de
817 Nefrología; 2015;35: 322–327. doi:10.1016/j.nefro.2015.05.002

818 42. Iozzo R V. MATRIX PROTEOGLYCANS: From Molecular Design to Cellular
819 Function. Annu Rev Biochem. 1998;67: 609–652.
820 doi:10.1146/annurev.biochem.67.1.609

821 43. Schaefer L, Gröne HJ, Raslik I, Robenek H, Ugorcakova J, Budny S, et al. Small

proteoglycans of normal adult human kidney: Distinct expression patterns of decorin, biglycan, fibromodulin, and lumican. Kidney Int. 2000;58: 1557–1568. doi:10.1046/j.1523-1755.2000.00317.x

44. Stokes MB, Holler S, Cui Y, Hudkins KL, Eitner F, Fogo A, et al. Expression of decorin, biglycan, and collagen type I in human renal fibrosing disease. Kidney Int. 2000;57: 487–498. doi:10.1046/j.1523-1755.2000.00868.x

45. Rosú SA, Toledo L, Urbano BF, Sanchez SA, Calabrese GC, Tricerri MA. Learning from Synthetic Models of Extracellular Matrix; Differential Binding of Wild Type and Amyloidogenic Human Apolipoprotein A-I to Hydrogels Formed from Molecules Having Charges Similar to Those Found in Natural GAGs. Protein J. 2017;36. doi:10.1007/s10930-017-9728-8

46. Raimondi S, Guglielmi F, Giorgetti S, Di Gaetano S, Arciello A, Monti DM, et al. Effects of the known pathogenic mutations on the aggregation pathway of the amyloidogenic peptide of apolipoprotein A-I. J Mol Biol. England; 2011;407: 465–476. doi:10.1016/j.jmb.2011.01.044

47. Gursky O, Mei X, Atkinson D. The Crystal Structure of the C-Terminal Truncated Apolipoprotein A-I Sheds New Light on Amyloid Formation by the N-Terminal Fragment. 2012;

48. Ramella NA, Andújar I, Ríos JL, Rosú SA, Tricerri MA, Schinella GR. Human apolipoprotein A-I Gly26Arg stimulation of inflammatory responses via NF-kB activation: Potential roles in amyloidosis? Pathophysiology. 2018; doi:10.1016/j.pathophys.2018.08.002

49. Scarpioni R, Obici L. Renal involvement in autoinflammatory diseases and inflammasome-mediated chronic kidney damage. Clin Exp Rheumatol. 2018;36: S54–S60.

847 50. Gustot A, Raussens V, Dehousse M, Dumoulin M, Bryant CE, Ruysschaert JM,
848 et al. Activation of innate immunity by lysozyme fibrils is critically dependent on
849 cross-β sheet structure. Cell Mol Life Sci. 2013;70: 2999–3012.
850 doi:10.1007/s00018-012-1245-5
851

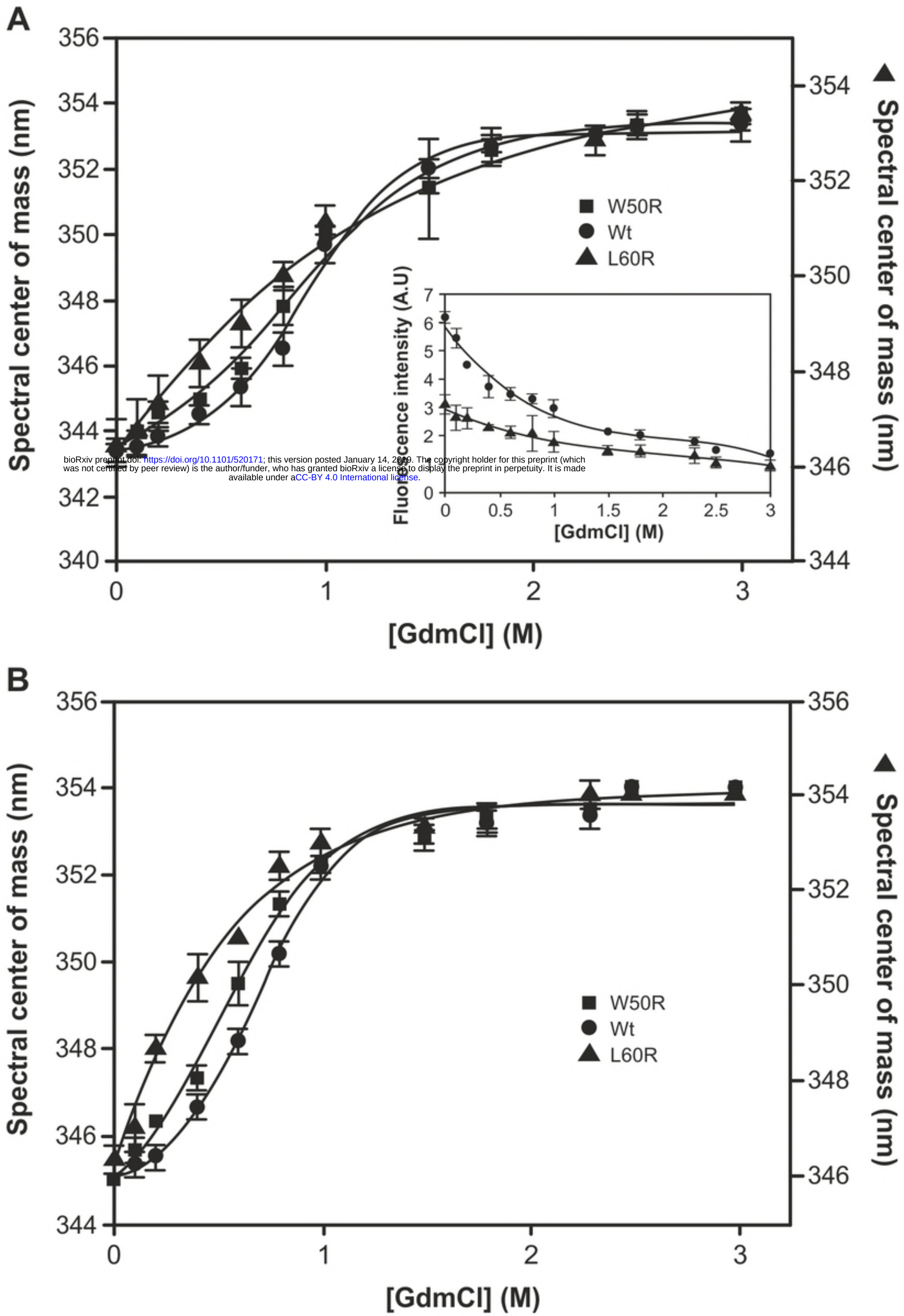

Figure 1 a-b

C

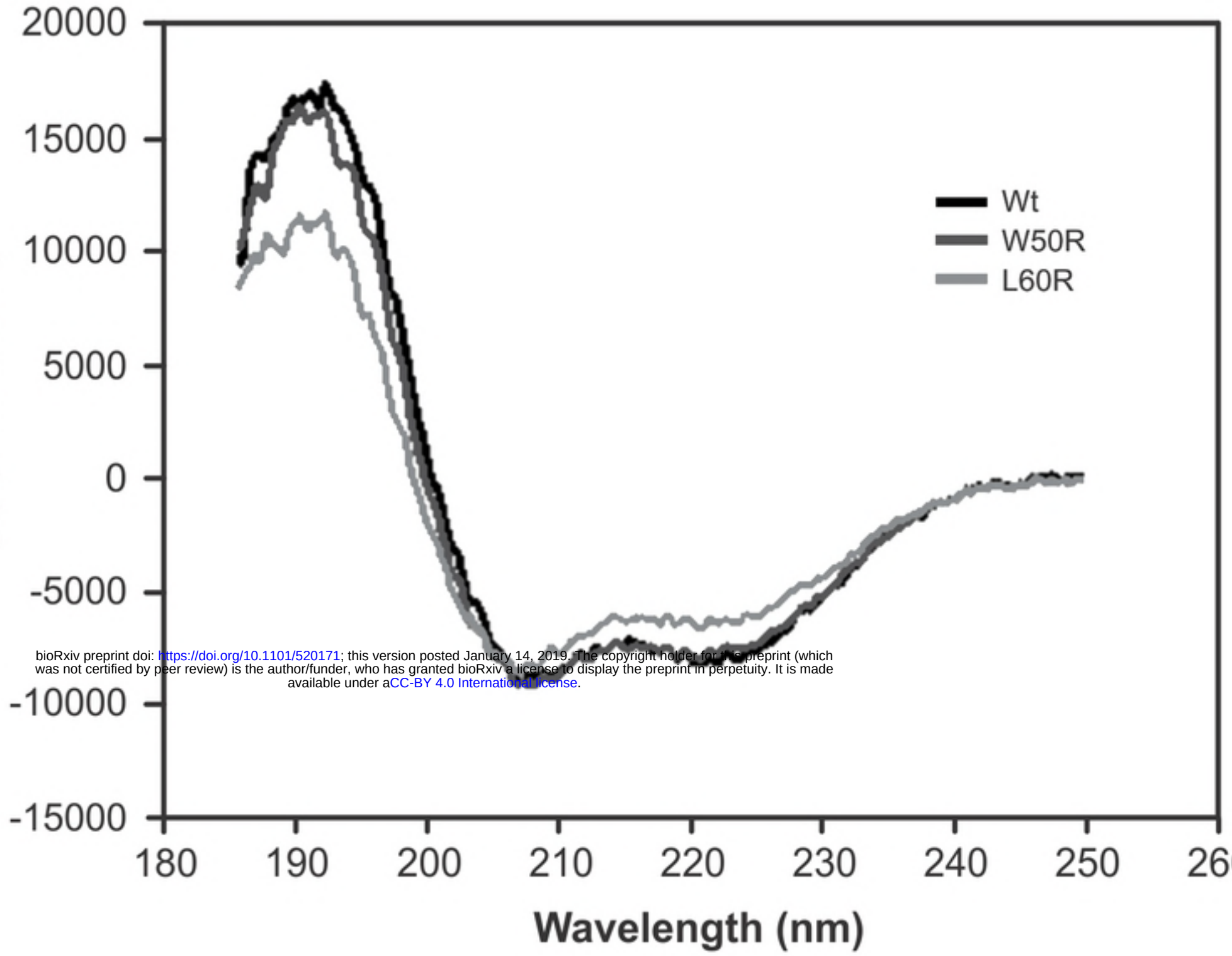

D

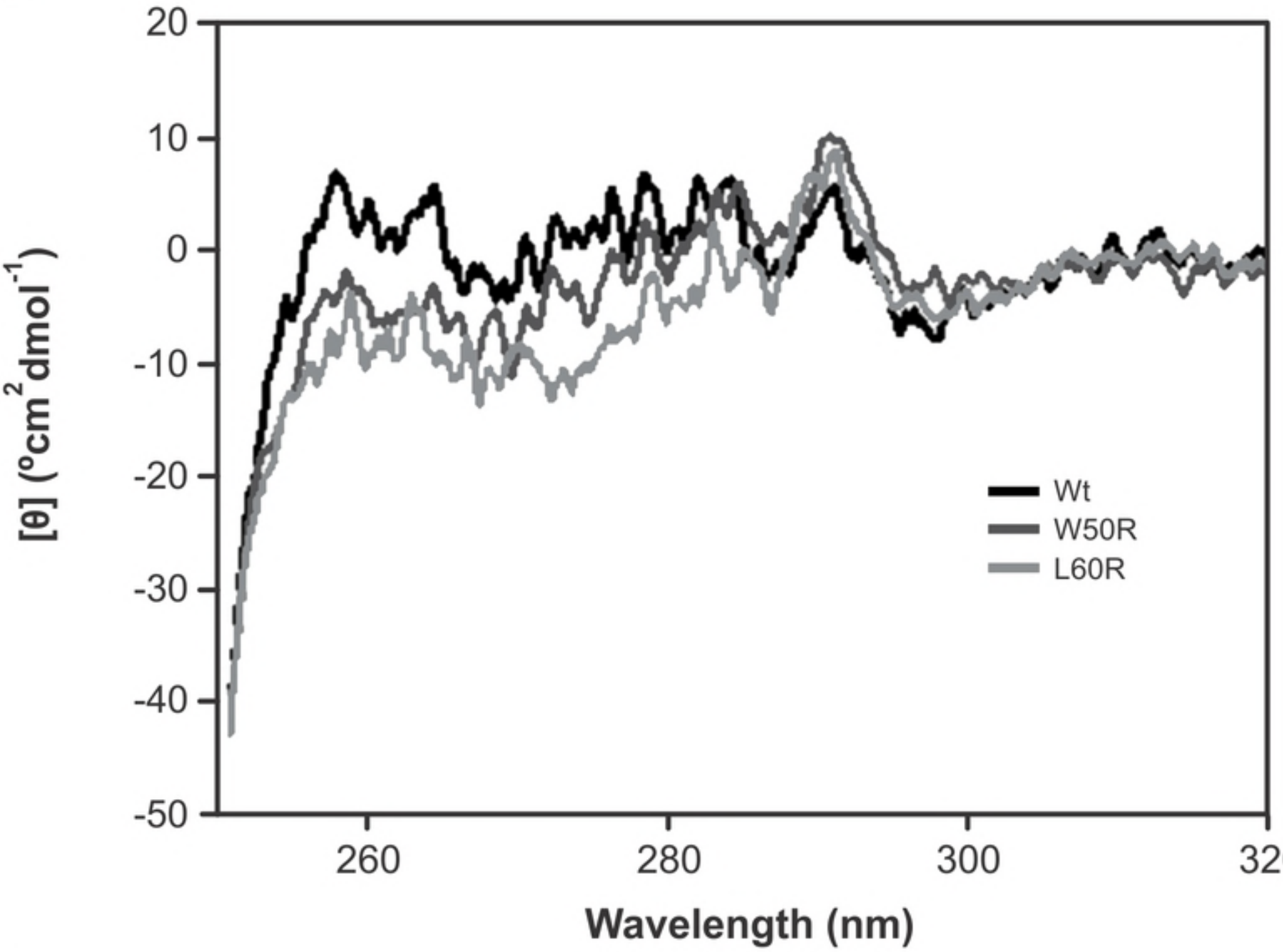

Figure 1 c-d

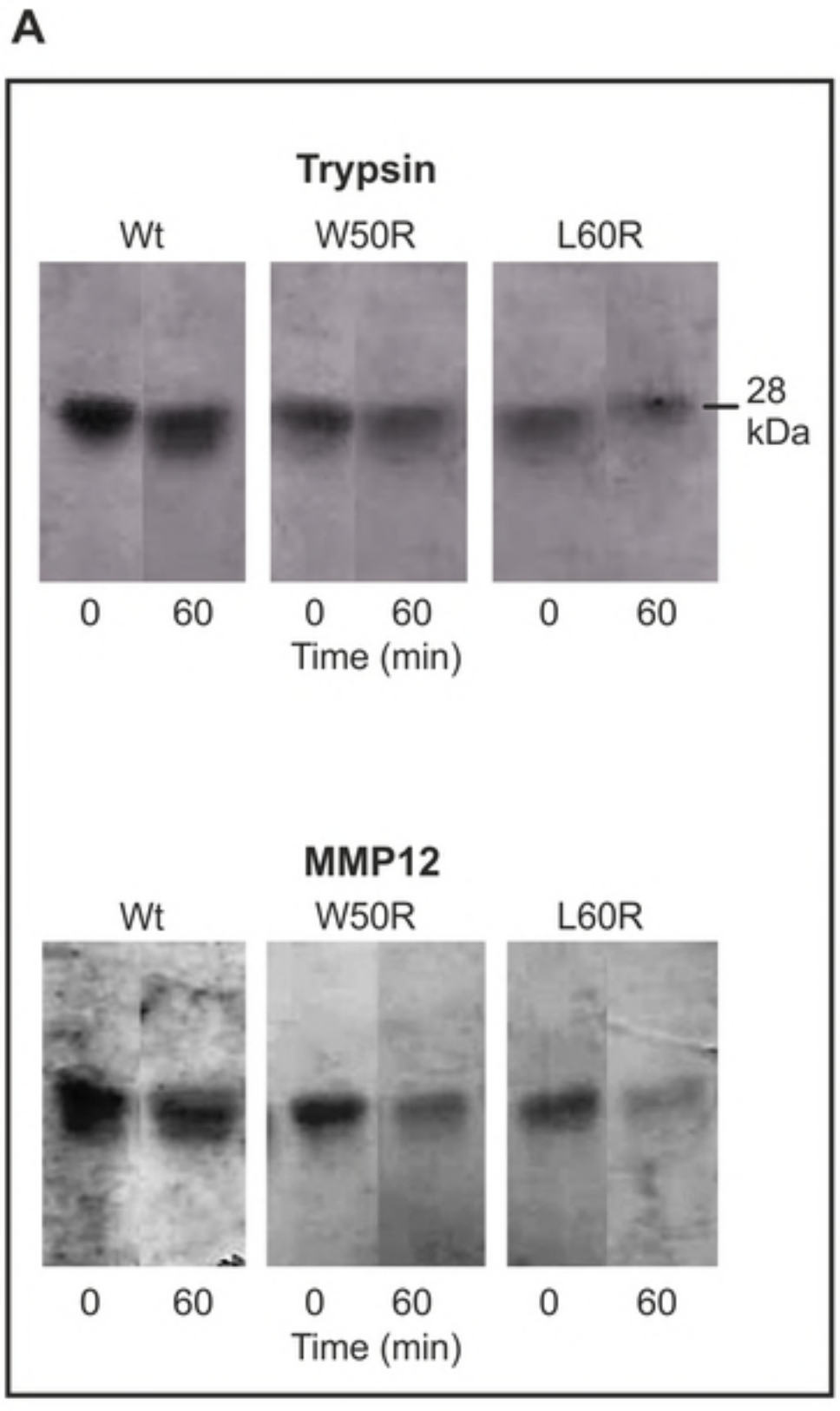
A
Trypsin
Wt
W50R
L60R
28 kDa
0 60 0 60 0 60
Time (min)
MMP12
Wt
W50R
L60R
0 60 0 60 0 60
Time (min)

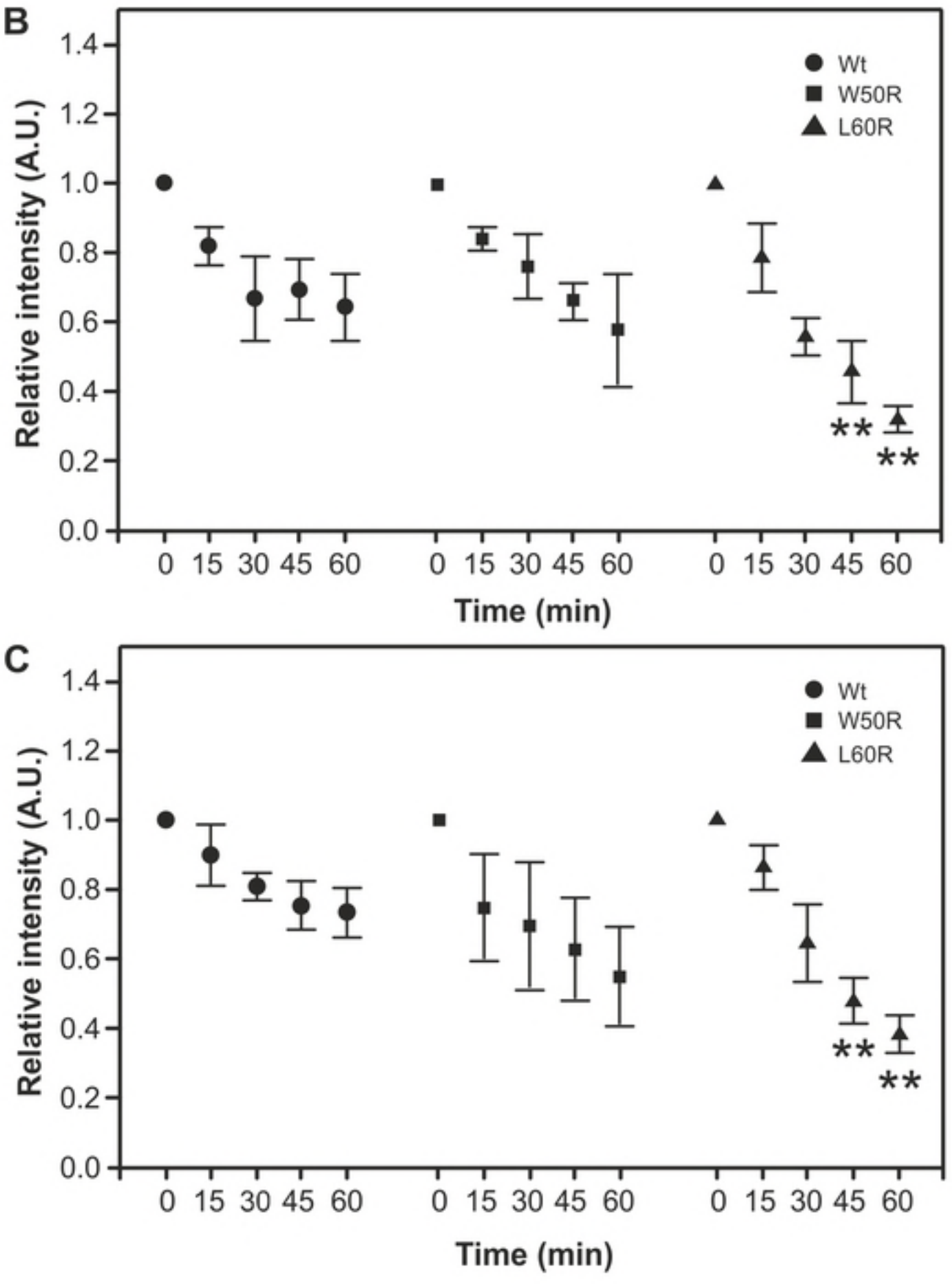
B
Relative intensity (A.U.)
1.4
1.2
1.0
0.8
0.6
0.4
0.2
0.0
Wt
W50R
L60R
**
**
0 15 30 45 60 0 15 30 45 60 0 15 30 45 60
Time (min)
C
Relative intensity (A.U.)
1.4
1.2
1.0
0.8
0.6
0.4
0.2
0.0
Wt
W50R
L60R
**
**
0 15 30 45 60 0 15 30 45 60 0 15 30 45 60
Time (min)

Figure 2

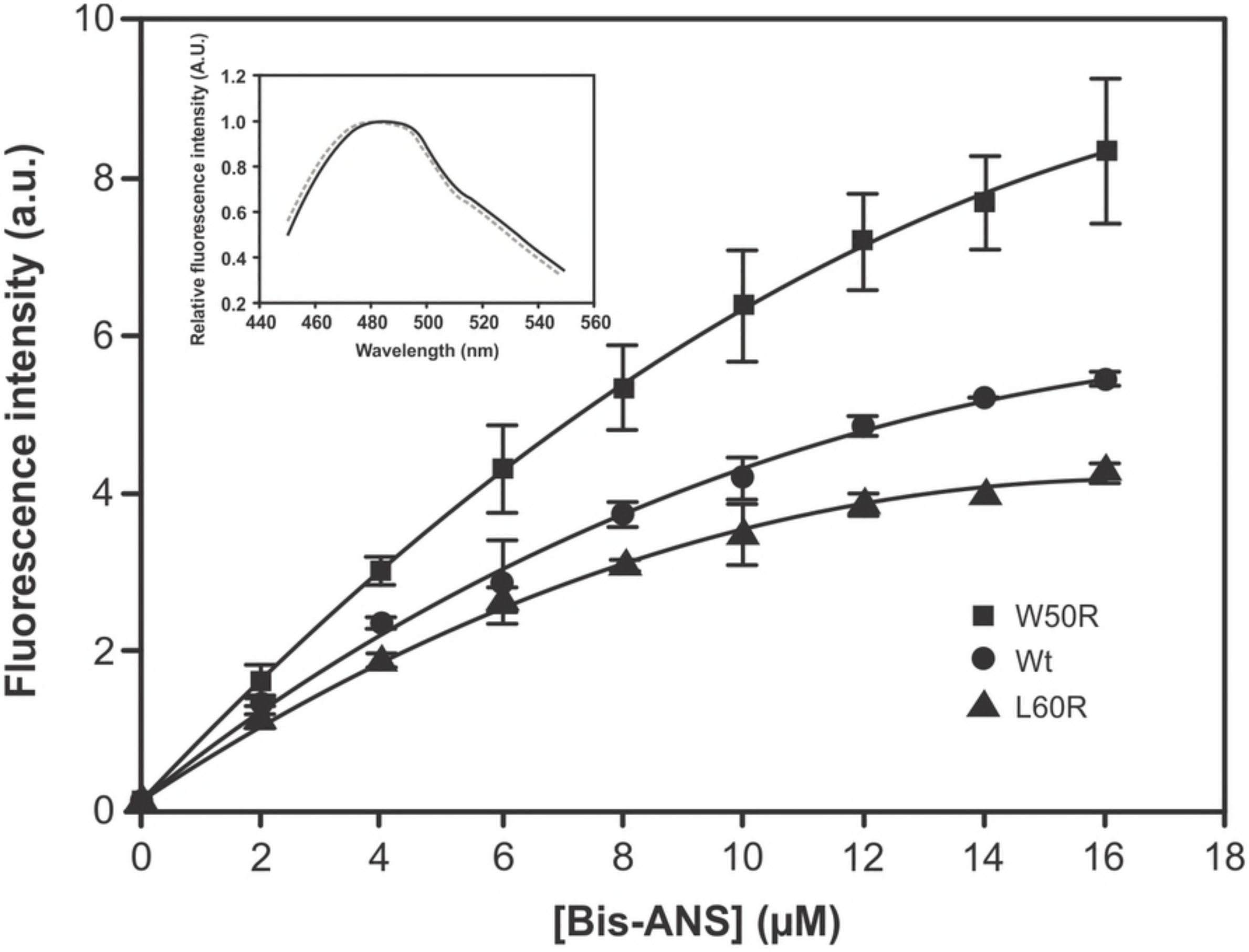
Fluorescence intensity (a.u.)
[Bis-ANS] (μM)
W50R
Wt
L60R
Relative fluorescence intensity (A.U.)
Wavelength (nm)

Figure 3

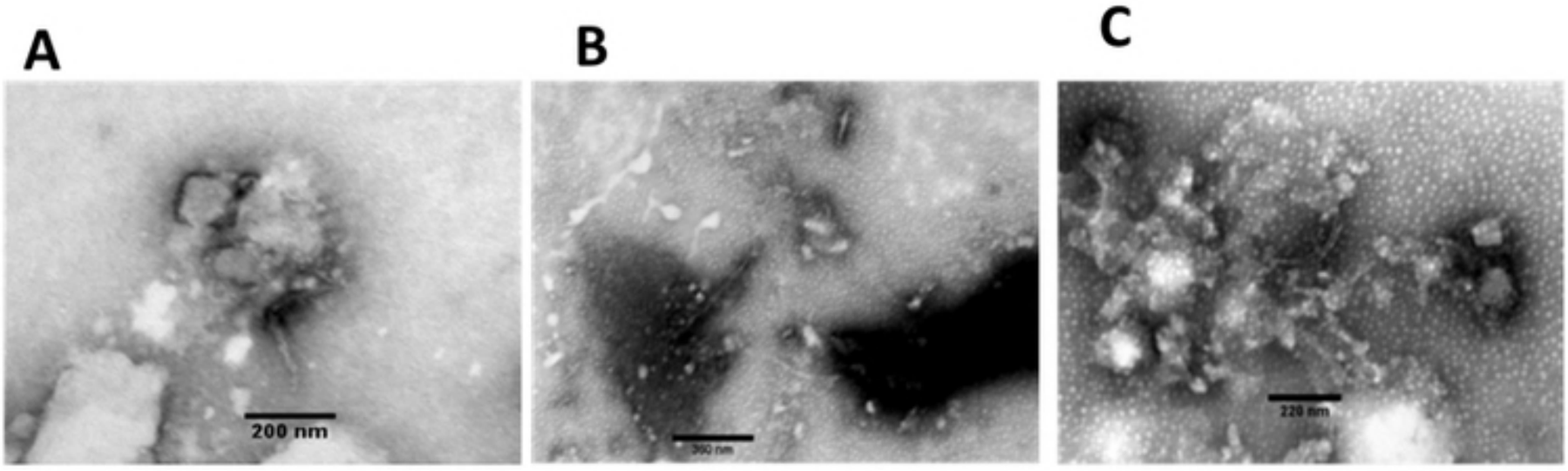

Figure 4

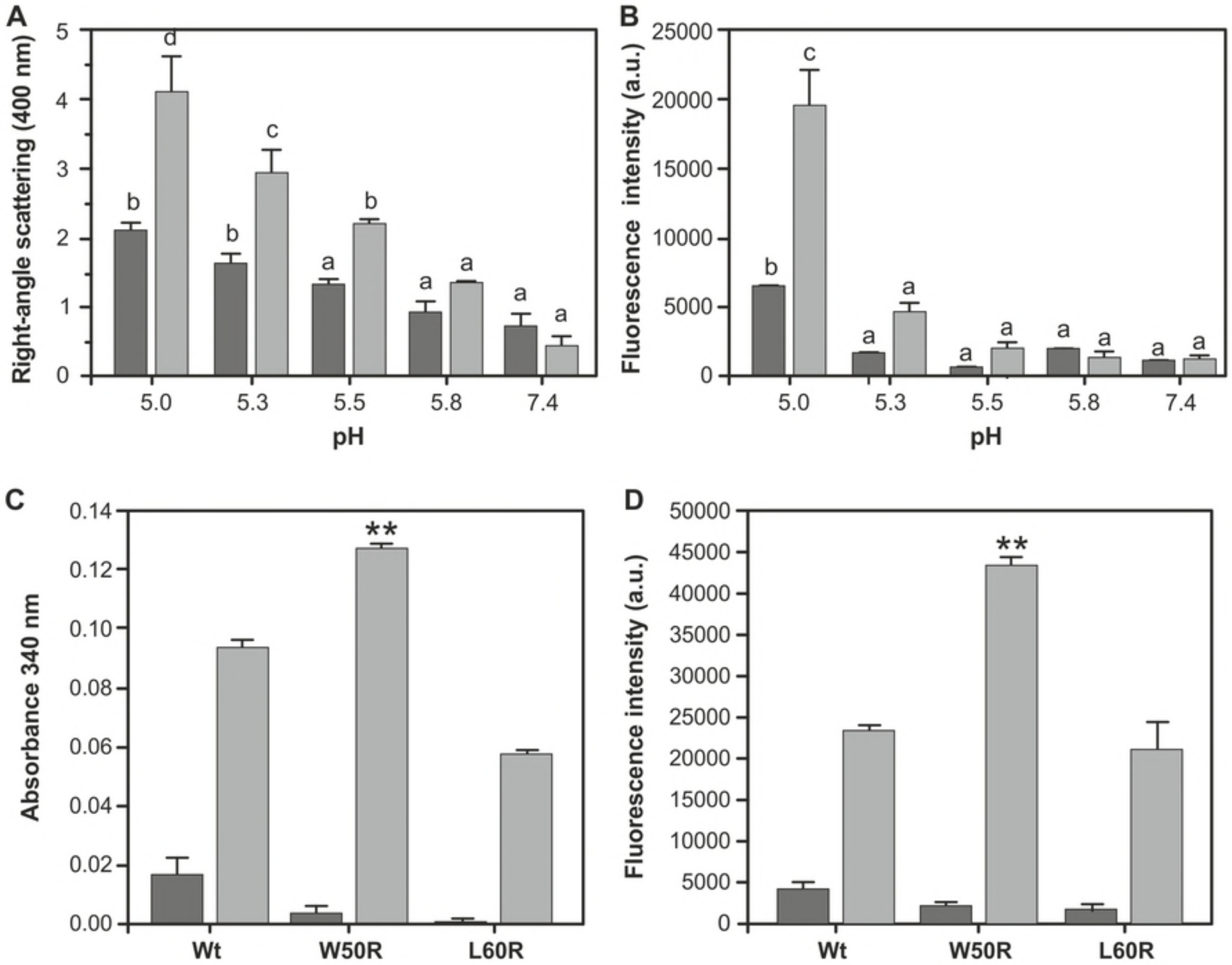
A
Right-angle scattering (400 nm)
0
1
2
3
4
5
b
d
b
c
a
b
a
a
a
a
5.0
5.3
5.5
5.8
7.4
pH
B
Fluorescence intensity (a.u.)
0
5000
10000
15000
20000
25000
b
c
a
a
a
a
a
a
a
a
5.0
5.3
5.5
5.8
7.4
pH
C
Absorbance 340 nm
0.00
0.02
0.04
0.06
0.08
0.10
0.12
0.14
**
Wt
W50R
L60R
D
Fluorescence intensity (a.u.)
0
5000
10000
15000
20000
25000
30000
35000
40000
45000
50000
**
Wt
W50R
L60R

Figure 5

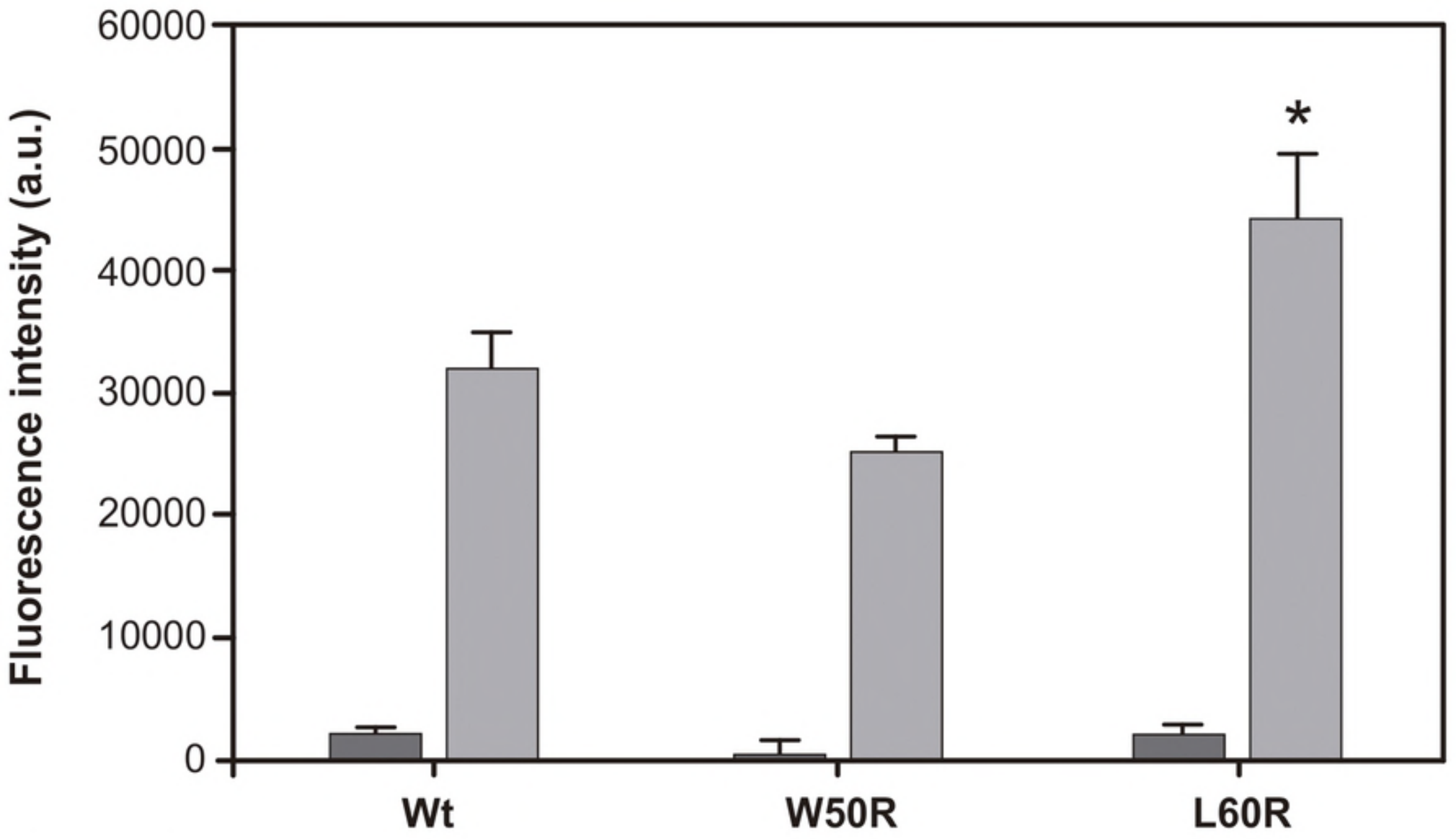
60000
50000
40000
30000
20000
10000
0
Fluorescence intensity (a.u.)
*
Wt
W50R
L60R

Figure 6

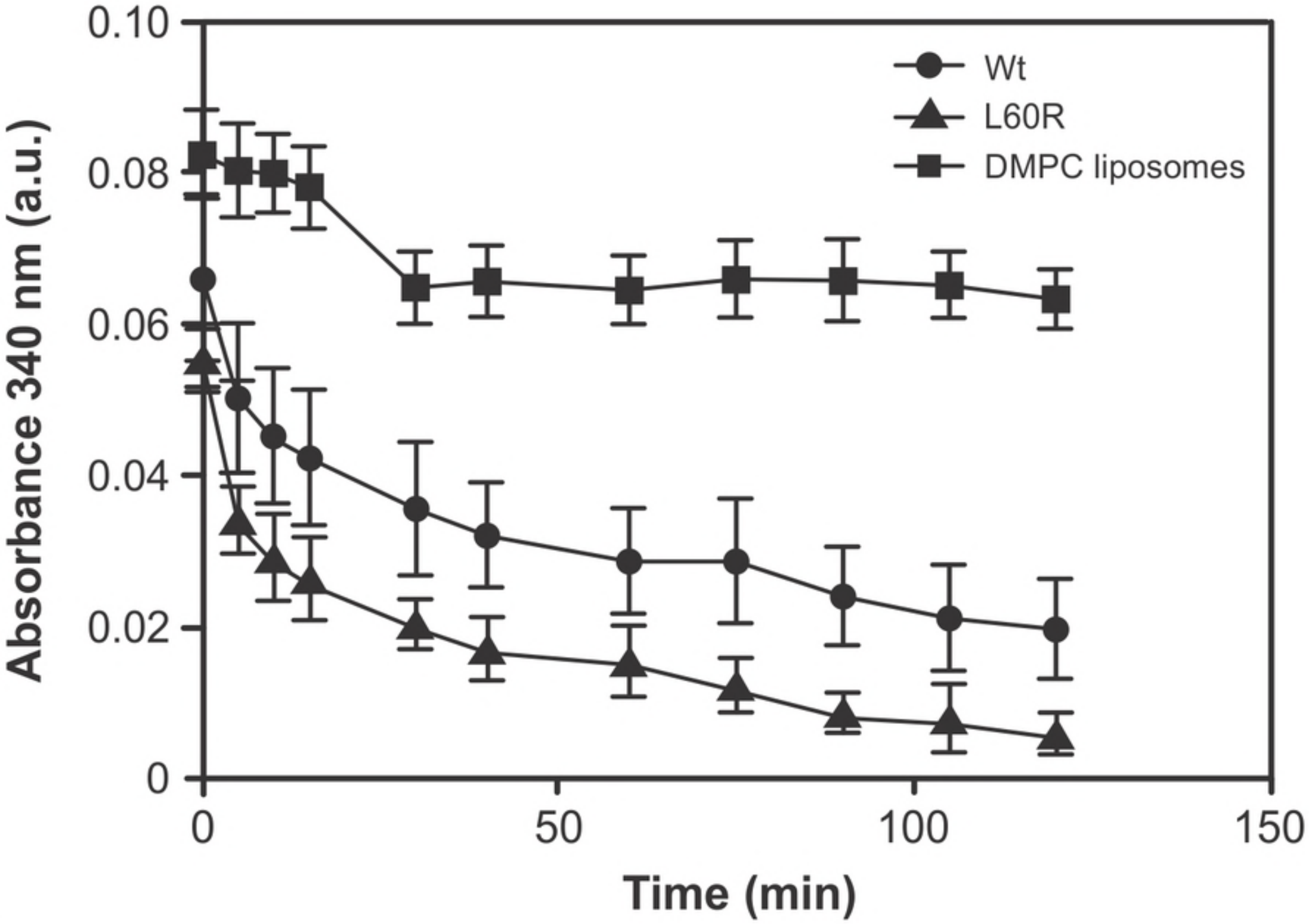
0.10
0.08
0.06
0.04
0.02
0
Absorbance 340 nm (a.u.)
0
50
100
150
Time (min)
Wt
L60R
DMPC liposomes

Figure 7

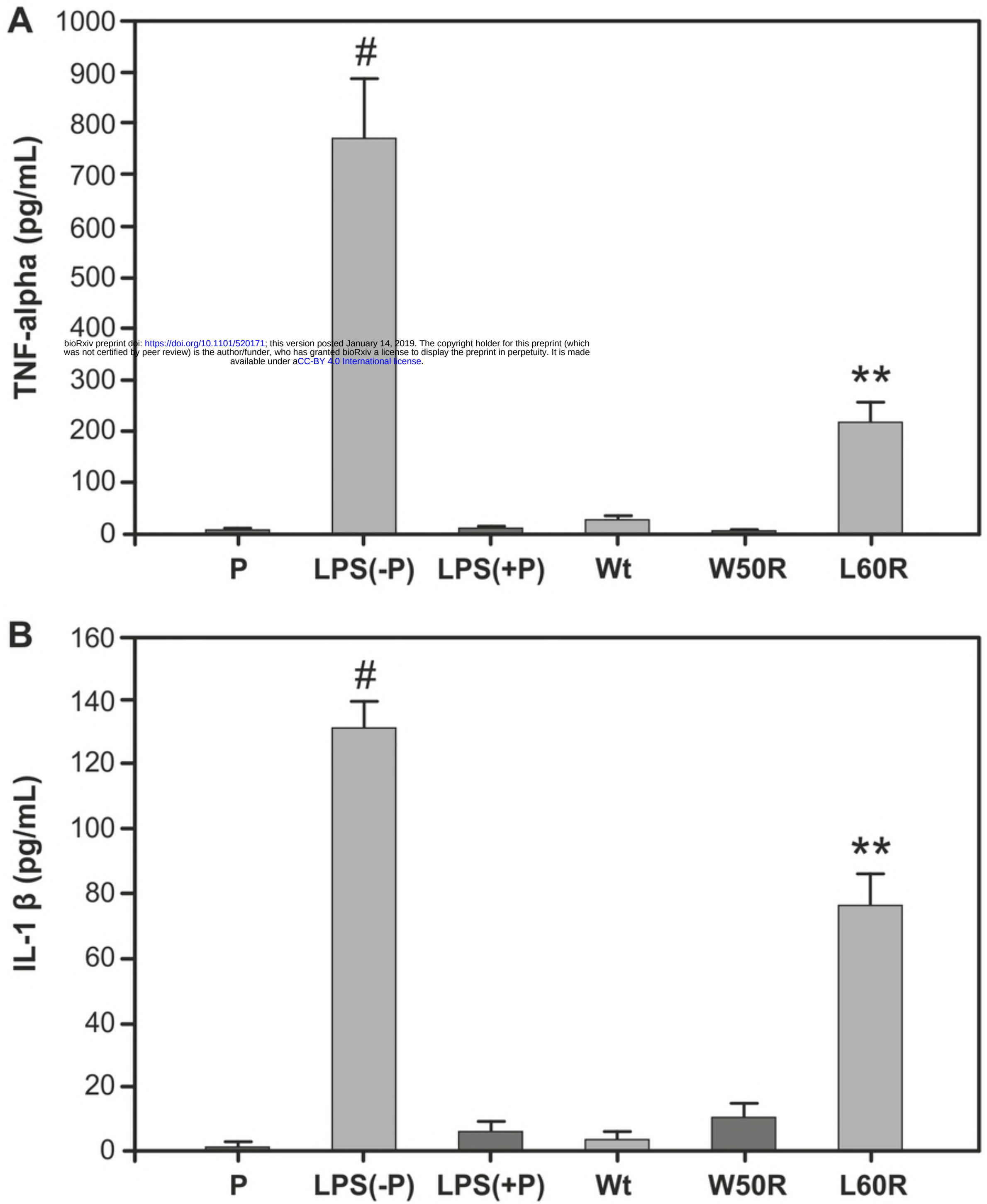

Figure 8

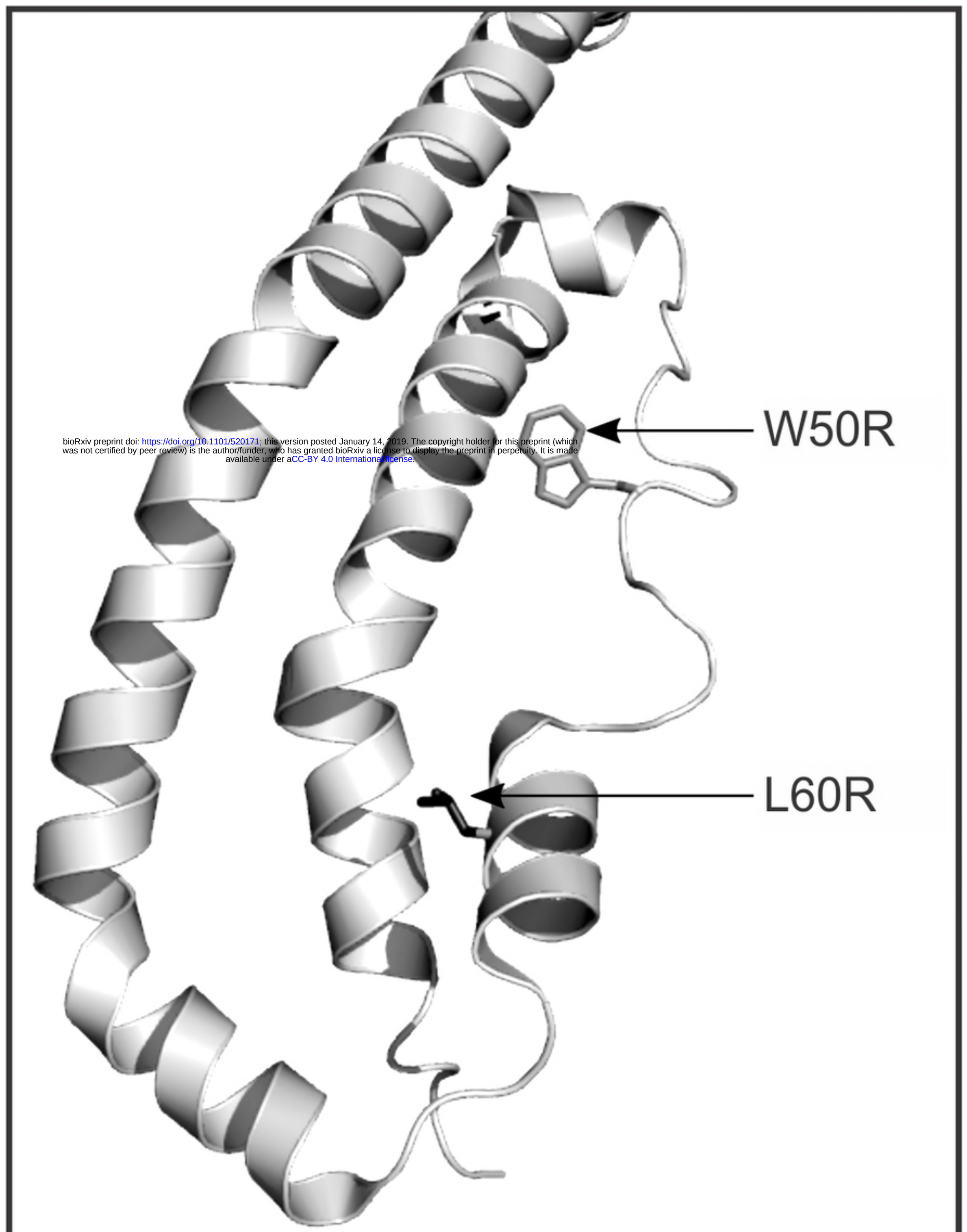

Figure 9

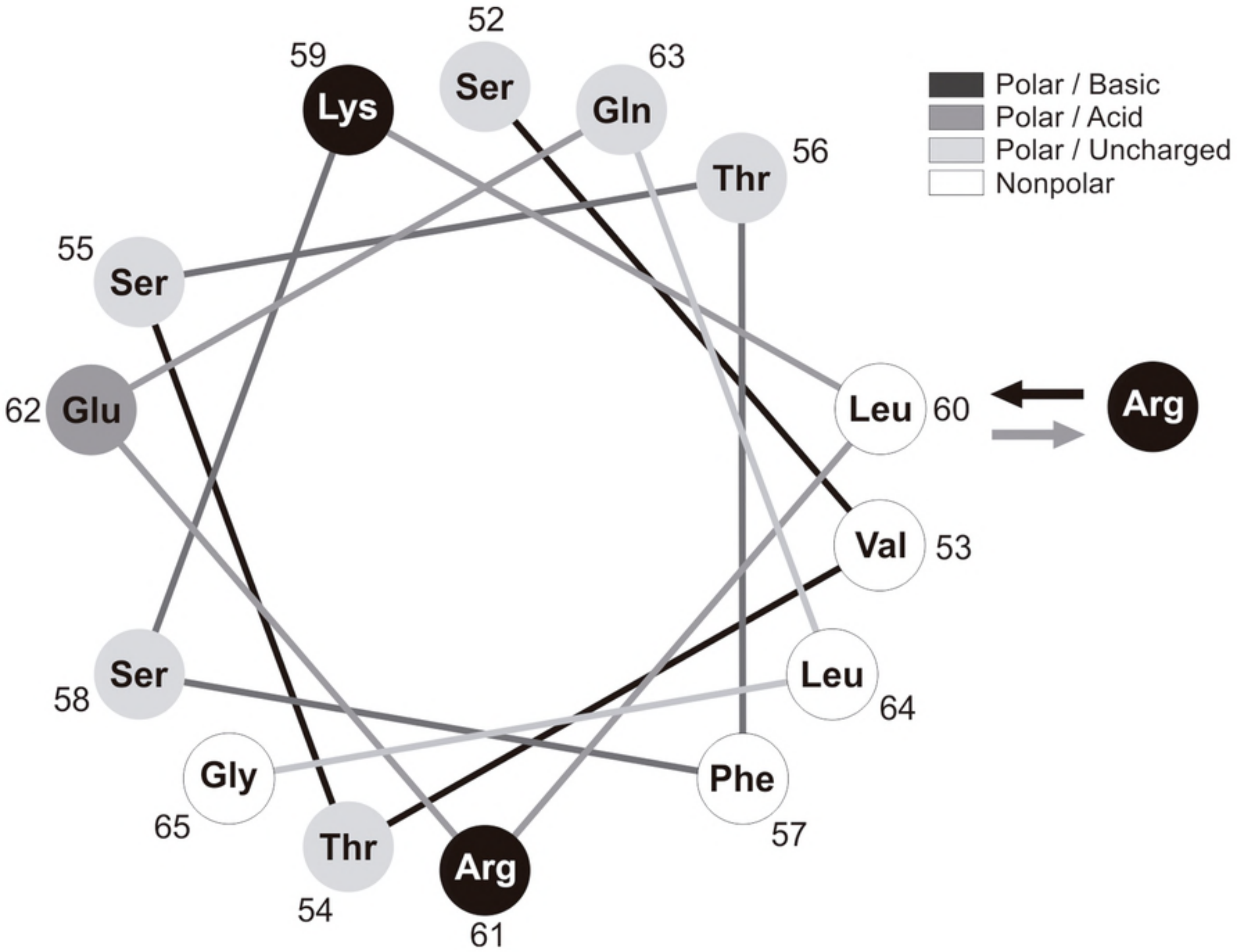
Polar / Basic
Polar / Acid
Polar / Uncharged
Nonpolar
52
Ser
59
Lys
63
Gln
56
Thr
55
Ser
62
Glu
Leu
60
Arg
Val
53
Ser
58
Leu
64
Gly
65
Phe
57
Thr
54
Arg
61

Figure 10